Published OnlineFirst May 30, 2013; DOI: 10.1158/0008-5472.CAN-13-0085

Flow cytometry

Peripheral blood mononuclear cell (PBMC) fractions derived from patients with colorectal cancer were stained for CD11b and Jag2. Briefly, 5×10^5 cells were blocked for 10 minutes at 4°C with FcR fragment in a 1:100 dilution and then incubated with anti-CD11b (APC anti-human CD11b, 301409 BioLegend) and Jag2 (PE anti-human Jag2, 346903 BioLegend) antibodies in a 2.5:100 dilution in PBS + BSA 0.5% for 45 minutes in the dark with rotation at 4°C. Characterization of tumor-associated bone marrow–derived cells was conducted by staining digested tumor samples for Jag2 (PE anti-mouse Jag2, 131007, BioLegend), CD11b (FITC anti-mouse CD11b, 101205 BioLegend), Gr-1 [APC/Cy7 anti-mouse Ly-6G/Ly-6C (Gr-1), 108423 BioLegend], F4/80 (FITC anti-mouse F4/80, 123107 BioLegend), Sca-1 (FITC anti-Mouse Ly-6A/E, 557405 BD Pharmingen), c-Kit [APC/Cy7 anti-mouse CD117 (c-kit), 105825, BioLegend], CD3 (FITC anti-mouse CD3, 100203 BioLegend), and CD19 (Alexa Fluor 488 anti-mouse CD19, 115524 BioLegend). Antibodies used were diluted 1:100 in PBS + BSA 0.5% and incubated in the dark with rotation at 4°C for 45 minutes. Flow cytometry was conducted on FACSCalibur and analyzed with FlowJo 8.7 Software (Tree Star, Inc. 1997–2012).

Quantitative reverse-transcription PCR

RNA extraction (TRIzol, Invitrogen) and cDNA synthesis [Reverse-transcription with Superscript II reverse transcriptase (Invitrogen)] were conducted following standard protocols. Reverse-transcription PCR (RT-PCR) was conducted with Power SYBR Green PCR Master Mix in 7900HT Fast Real-Time PCR System (both from Applied Biosystems). Primer sequences for hE-Cadherin, hVimentin, hHey1, hHey2, mDll1, mDll4, mJag1, and mJag2 are shown in Table 2. The housekeeper gene used to normalize human samples was *h18s* and to normalize mouse samples was *m18s*. RT-PCR data were analyzed by DataAssist software (Applied Biosystems).

Tumor histocytochemistry procedure and analysis

Human colorectal cancer tumor paraffin-included samples were provided by the Pathology department at IPO-Lisboa. Samples were serially sectioned (3 μm), adsorbed into slides and then subjected to antigen retrieval (PT Link, Dako). After being deparaffinized, sections were blocked in PBS + 10% goat serum for 30 minutes at room temperature and then incubated with primary antibody at room temperature for 1 hour. Counterstaining was conducted using Mayer hematoxylin. Serial sections were stained for Jag2 (sc-56041 Santa Cruz, 1:15), CD11b (HPA002274 Sigma, 1:300), E-cadherin (18-0223 Invitrogen, 1:50), and cytokeratin-19 (CK19; M0888 Dako, 1:50). Slides were analyzed and photographed in a Leica DMD108 microscope. Concerning $CD11b^+$ $Jag2^+$ cell quantification, tissue sections were screened at low power field (×100 magnification), and the 10 areas with the most intense staining for CD11b (hot spots) were selected. Jag2 staining in these areas was confirmed in the serial slide. Counts of the hot spots were conducted at high power field (HPF; ×400). The mean number of positive cells in the 10 hot spot areas was expressed for each condition. E-cadherin quantification on each slide was conducted using the ImmunoMembrane software version 1.0i (16). Results were further validated by a pathologist at IPO-Lisboa. Mouse tumors samples were included in either gelatin or paraffin. Paraffin tumor sections were further subjected to antigen retrieval protocols (PT high). Tumor cryosections were blocked with a 5% FBS/0.1% BSA solution in PBS for 30 minutes. Slides were then covered with primary antibodies: anti-mouse PECAM (553369, Pharmingen), anti-mouse CD11b (550282, Pharmingen), anti-human E-cadherin (M3612, Dako); anti-human CK19 (M0888, Dako), anti-human (M0851, Dako), anti-human C-Kit (A4502, Dako), anti-mouse B220 (553085, Pharmingen), and anti-human Jag2 (AbCam). After overnight incubation at 4°C, tumor sections were washed in PBS and incubated with secondary antibodies from Invitrogen (anti-rat-FITC, anti-mouse-Alexa568, anti-rabbit-Alexa488, respectively) for 2 hours at room temperature. For the quantification of GFP^+ lineage+ cells in tumor samples, the total number of GFP^+ lineage+ cells was quantified in 5 HPFs (×400) and then divided by total GFP^+ cells. Quantification of vimentin+ cells was preformed by direct count of vimentin-expressing cells in 5 HPFs (×400). Quantification of E-cadherin expression on tumor samples was performed by direct quantification of staining intensity and area using ImageJ software.

Statistical analysis

Results are expressed as mean ± SEM. Data were analyzed with GraphPad software (GraphPad Software, Inc; v4.0b) using unpaired two-tailed student *t* test or Mann–Whitney test when indicated. *P* values of less than 0.05 were considered statistically significant.

Results

Bone marrow–derived cells infiltrate ectopic colorectal tumors and localize in regions undergoing EMT

To characterize the contribution of bone marrow–derived cells during colorectal cancer progression, we started by inoculating HCT15 (human colon carcinoma cell line) subcutaneously into nude mice that had been transplanted with actin-GFP^+ BM (Supplementary Fig. S1). Tumors were allowed to grow for 1 to 3 weeks (termed early and late tumors, respectively), after which the mice were sacrificed and tumors collected. As shown in Fig. 1, bone marrow–derived cells (GFP^+ cells) actively infiltrate early and late tumors, and are found at higher frequency in late tumors (Fig. 1A). We also observed that as tumors grew, there was a significant decrease in E-cadherin expression and a significant increase in the expression of the mesenchymal marker vimentin (Fig. 1B and C), suggestive of EMT. Considering that bone marrow–derived cells' infiltration into tumors and EMT were associated with tumor growth, we analyzed possible correlations between GFP^+ cell infiltration and E-cadherin and vimentin expression in tumor tissues. There was an inverse correlation ($P = 0.0097$; $R^2 = 0.7678$, 7 samples) between GFP^+ and E-cadherin+ areas, but a direct correlation ($P = 0.0297$; $R^2 = 0.6448$, 7 samples) between GFP^+ areas and the number of vimentin+ cells in tumor tissues (Fig. 1D). Detailed observation of tumor sections showed that CK19-positive tumor cells in close proximity with GFP^+ cells acquire the expression of vimentin, while tumor cells further away do not (Fig. 1E, bottom, white arrows). Consistent with the EMT

Published OnlineFirst May 30, 2013; DOI: 10.1158/0008-5472.CAN-13-0085

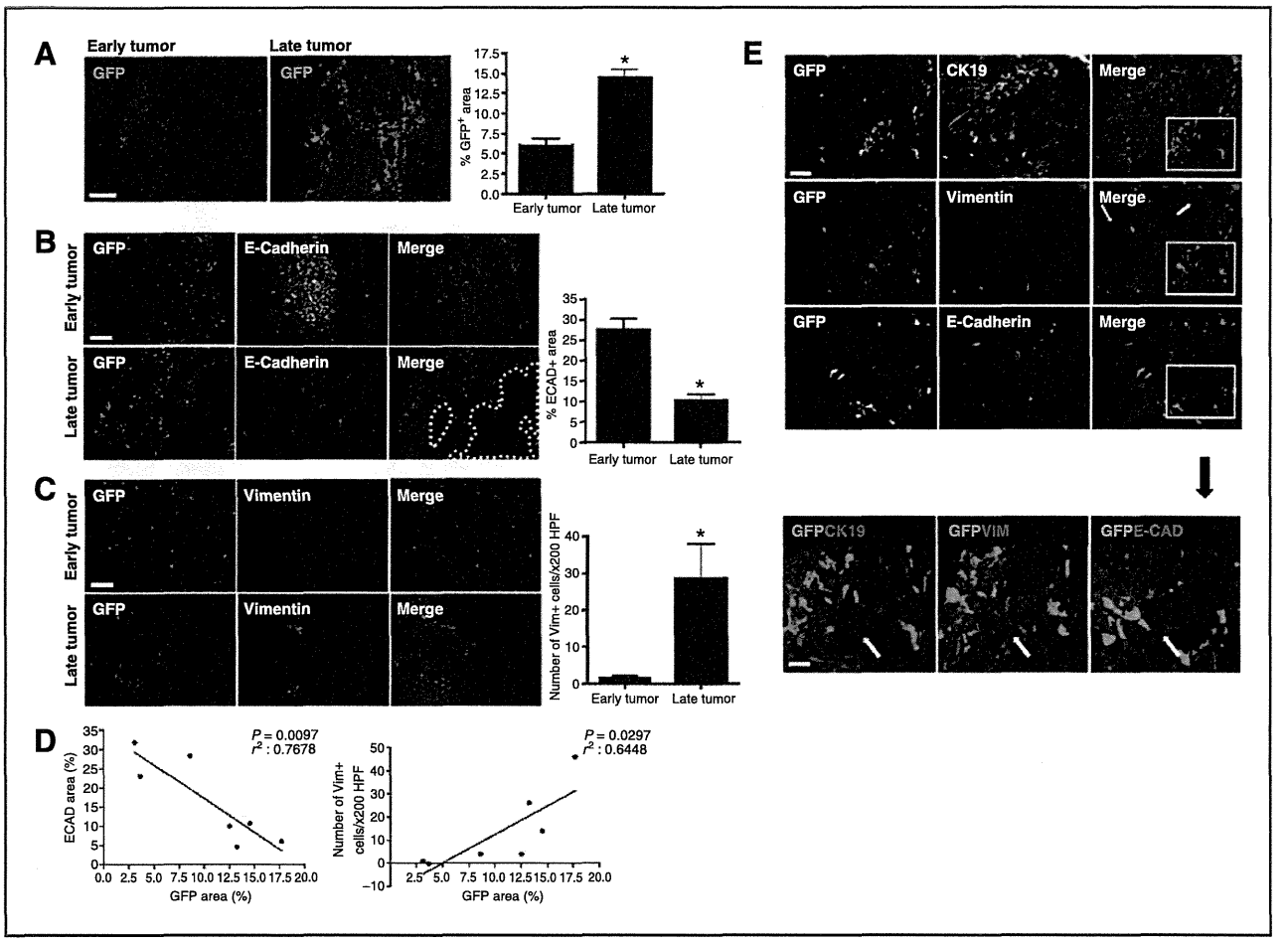

Figure 1. Bone marrow–derived cells infiltrate ectopic colorectal tumors and localize in regions undergoing EMT. A, representative image of early (1 week) and late (3–4 weeks) subcutaneous colon tumors implanted into GFP$^+$ BM nude mice. Scale bar, 100 μm. Quantification of the GFP area percentage in both early and late tumors using ImageJ software. B, representative image of GFP (green) and E-cadherin (red) expression on early and late colon tumors. Dashed line delimitates tumor regions that show decreased E-cadherin (ECAD) expression. Scale bar, 100 μm. Quantification of the E-cadherin area percentage in both early and late tumors using ImageJ software. C, representative image of GFP (green) and vimentin (red) expression on early and late tumors. Scale bar, 100 μm. Quantification of the number of vimentin + cells in both early and late tumors using ImageJ software. D, correlation plot between E-cadherin area percentage and GFP area percentage (on the left) and also between the number of vimentin + cells and GFP area percentage (on the right). E, representative image of sequential tumor sections of the same region stained for GFP and CK19, GFP and vimentin, and GFP and E-cadherin. Arrows point to tumor cells (CK19+) in close contact with GFP cells that acquire vimentin expression and lose E-cadherin expression. Scale bar, 10 μm. Data are means ± SEM, *, $P < 0.05$; $n = 7$ (3 mice in early tumor group and 4 in late tumor group).

phenotype, tumor cells in proximity of GFP$^+$ cells also show decreased E-cadherin expression (Fig. 1E bottom right, white arrow). These data suggest that colorectal cancer growth is associated with an increased frequency of bone marrow–derived cells infiltration, which in turn correlate with the onset of EMT. Considering this, we hypothesized bone marrow–derived cells could induce EMT on epithelial tumor cells.

Bone marrow–derived cells induce EMT on colorectal carcinoma cells in a Notch pathway-dependent manner

To test the ability of bone marrow–derived cells to induce EMT on tumor cells, we conducted *in vitro* coculture experiments with HCT15 cells and bone marrow–derived (GFP$^+$) cells isolated (sorted out) from late subcutaneous tumors. As depicted in Fig. 2A in the presence of bone marrow–derived (GFP$^+$) cells isolated from tumors (TGFP+ cells), HCT15 lose E-cadherin expression and gain vimentin expression, as measured by quantitative RT-PCR (qRT-PCR). This can also be observed in the quantification of E-cadherin–expressing HCT15 cells by immunostaining after coculture (Fig. 2B), suggesting that TGFP+ cells induce vimentin expression and decrease E-cadherin expression at both transcriptional and translational level. Next, we looked into the molecular pathways regulating EMT induced by TGFP+ cells. The TGF-β and the Notch signaling pathways (19) have been implicated in EMT, thus we tested whether these pathways could be involved in bone marrow–derived cell-induced EMT on colon carcinoma cells. In agreement, we conducted coculture assays by adding a TGF-β blocking antibody and a Notch pathway inhibitor (GSI) and determined its effect on HCT15 cells E-cadherin and vimentin expression. TGF-β inhibition had no effect (data not shown), whereas addition of GSI inhibited the

Published OnlineFirst May 30, 2013; DOI: 10.1158/0008-5472.CAN-13-0085

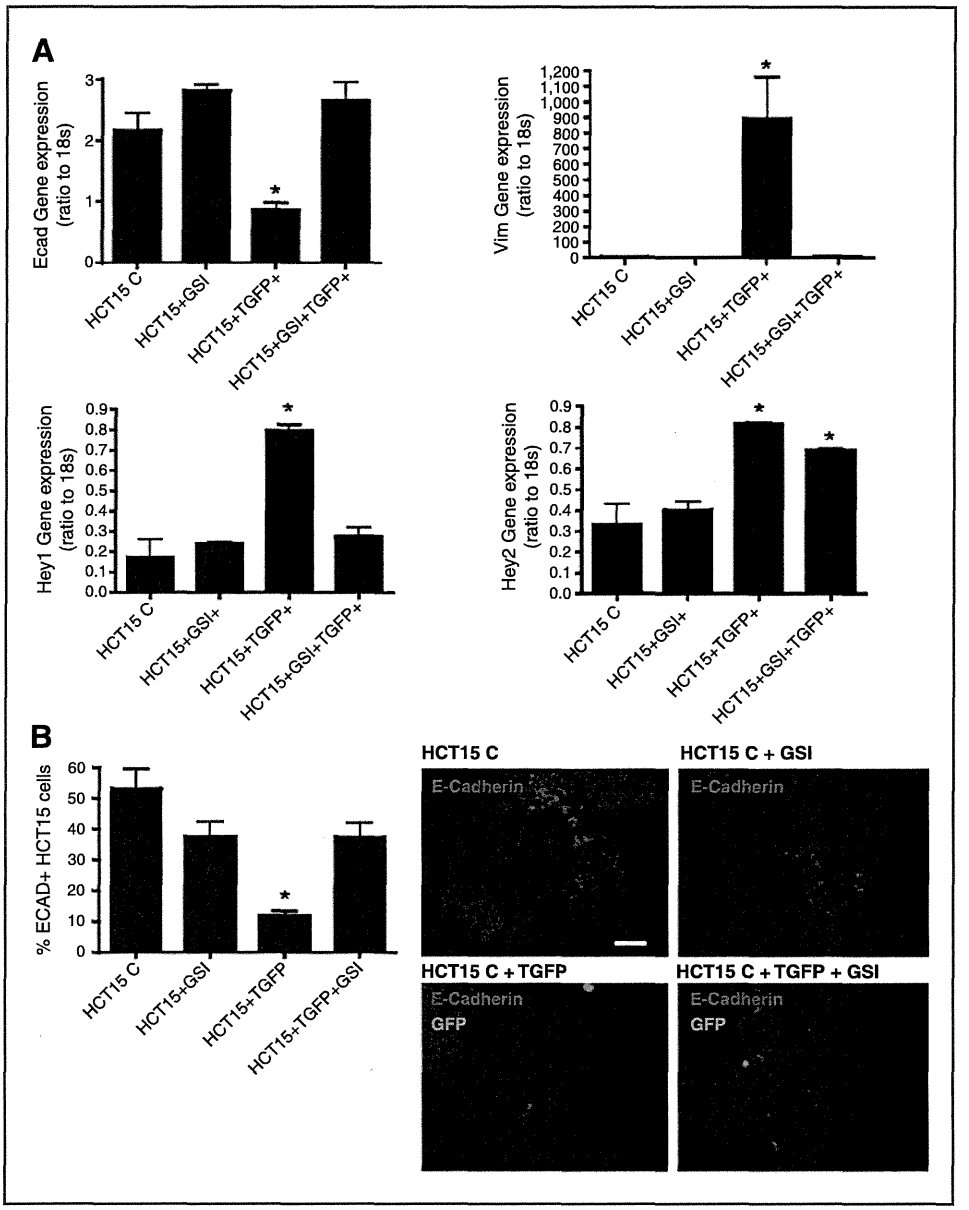

Figure 2. Bone marrow–derived cells induce EMT on colon carcinoma cells in a Notch pathway-dependent manner. A, quantification of E-cadherin, vimentin, Hey 1, and Hey 2 gene expression (normalized to 18s rRNA expression) by qRT-PCR on HCT15 alone (HCT15 C), in the presence of 10 μmol/L GSI (HCT15 + GSI), in the presence of bone marrow–derived cells isolated from the tumors (HCT15 + TGFP) alone, or in the presence of 10 μmol/L GSI (HCT15 + TGFP + GSI). B, quantification of E-cadherin+ HCT15 cells on HCT15 C, HCT15 + GSI, HCT15 + TGFP, and on HCT15 + TGFP + GSI coculture conditions. Representative images of E-cadherin (red) expression in HCT15 cells cocultured with bone marrow–derived cells isolated from the tumors (GFP^+; green). Data shown are means ± SEM of 3 independent experiments ($n = 3$), *, $P < 0.05$. Scale bar, 50 μm.

TGFP+ cell-induced decrease in E-cadherin and increase in vimentin expression (Fig. 2A). Furthermore, confirming the involvement of the Notch pathway is the observation that HCT15 cells express Notch receptors 1 and 4 (data not shown) and more importantly the Notch pathway downstream targets Hey 1 and 2 are upregulated in HCT15 cells undergoing EMT, in the presence of TGFP+ cells (Fig. 2A). These data suggest that bone marrow–derived cells induce EMT via Notch pathway activation on tumor cells.

Bone marrow–derived cells expressing Jag2 induce EMT on colorectal cancer cells

Having shown TGFP+ cells induce EMT on HCT15 cells and that this process involved Notch pathway activation, next we determined which ligands of the Delta:Notch family were expressed by the tumor-infiltrating bone marrow–derived cells. We determined and compared the expression of the ligands Delta-like ligand 1 (Dll1), 4 (Dll4), and Jag1 and 2 (Jag1, Jag2) in bone marrow–derived cells (GFP^+) collected from late tumors and from the corresponding bone marrow samples. Jag2 was the most abundantly expressed ligand on TGFP+ cells, its expression being significantly higher on TGFP+ cells than on those isolated from bone marrow (Fig. 3A). Detailed flow cytometry analysis of tumor and bone marrow samples of tumor-bearing mice revealed a population of GFP^+ $Jag2^+$ cells in both tissues, although at a higher frequency in the tumors, representing an average of 5.5 ± 1.12% cells (Fig. 3B). Taking into account the high frequency of GFP^+ Jag+ cells in tumors, next we investigated whether this population was able to induce EMT on HCT15 colon

Published OnlineFirst May 30, 2013; DOI: 10.1158/0008-5472.CAN-13-0085

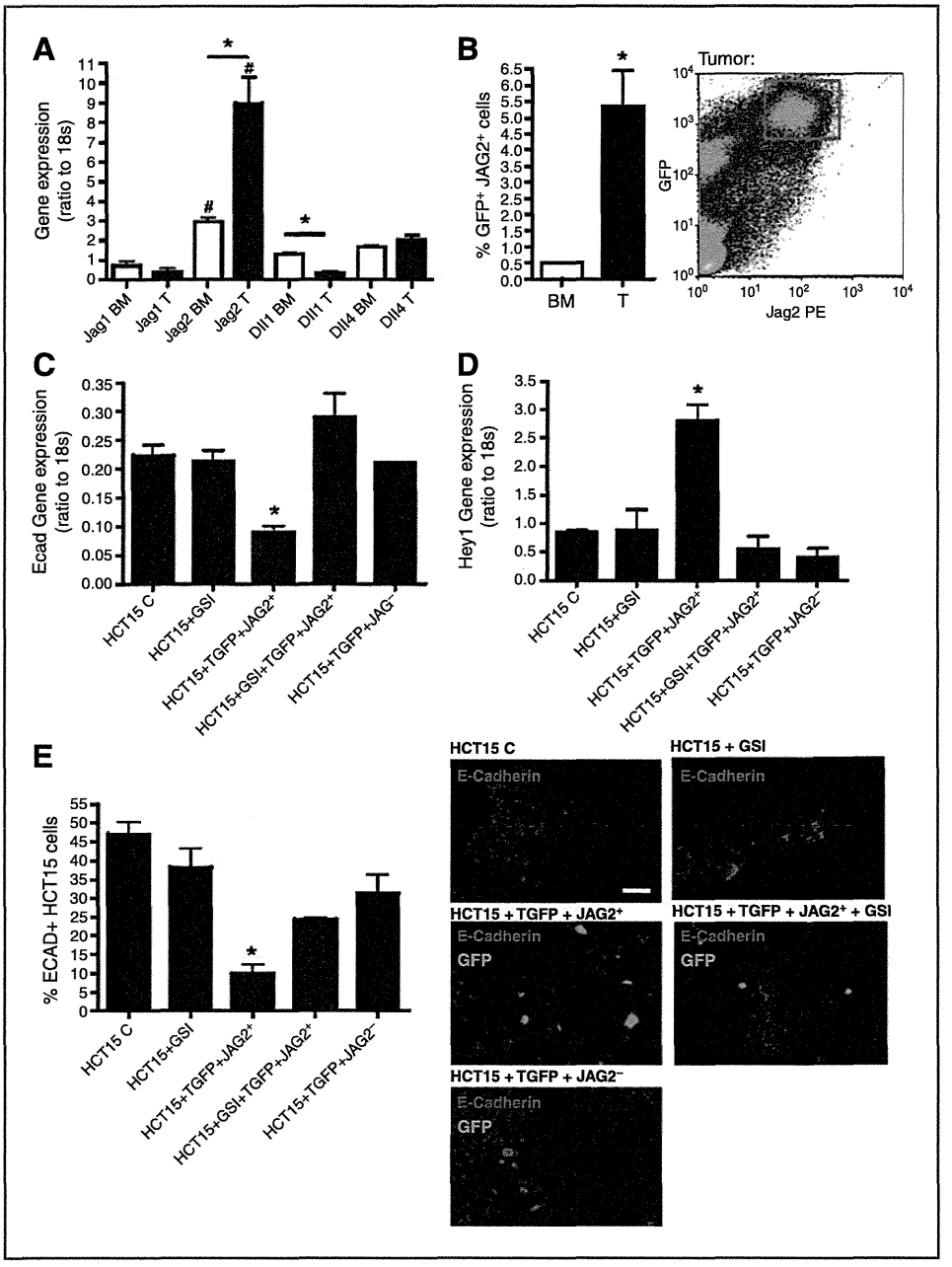

Figure 3. Bone marrow–derived cells expressing Jag2 induce EMT on colorectal cancer cells. A, Jag1, Jag2, Dll1, and Dll4 gene expression (normalized to 18s rRNA expression), determined by qRT-PCR in GFP$^+$ cells collected from tumors or bone marrow samples. Data shown are means ± SEM of 3 independent experiments ($n = 3$); *, $P < 0.05$ (between indicated groups); #, $P < 0.05$ (between gene expression in bone marrow or tumor samples). B, quantification of the percentage of GFP$^+$ Jag2$^+$ cells in bone marrow and tumor samples. Representative flow cytometry plot showing Jag2$^+$ bone marrow (BM)–derived cells in tumor (T) sample. C and D, quantification of E-cadherin (C) and Hey 1 gene expression (normalized to 18s rRNA expression; D) by qRT-PCR on HCT15 alone (HCT15 C), in the presence of 10 μmol/L GSI (HCT15 + GSI), in the presence of tumor associated bone marrow–derived Jag2$^+$ cells (HCT15 + TGFP-Jag2$^+$), in the presence of 10 μmol/L GSI and tumor-associated bone marrow–derived Jag2$^+$ cells (HCT15 + TGFP + Jag2$^+$ + GSI), or in the presence of tumor associated bone marrow–derived Jag2–negative cells (HCT15 + TGFP-Jag2$^-$). E, quantification of E-cadherin+ cells on HCT15 C, HCT15 + GSI, HCT15 + TGFP + Jag2$^+$, HCT15 + TGFP-Jag2$^+$ + GSI, or HCT15 + TGFP-Jag2- (negative) conditions. Panel shows representative images of E-cadherin (red) expression in HCT15 cells alone or in the different coculture conditions. Bone marrow–derived Jag2$^+$ cells isolated from the tumors are GFP$^+$ (green). Data shown are means ± SEM of 3 independent experiments ($n = 3$), *, $P < 0.05$. Scale bar, 50 μm.

carcinoma cells. GFP$^+$ Jag2$^+$, and also GFP$^+$ Jag2$^-$ cells were sorted from late tumors (Fig. 3B) and cocultured with HCT15 in the presence or absence of GSI. As depicted in Fig. 3C and D, GFP$^+$ Jag2$^+$ but not GFP$^+$ Jag2$^-$ cells were able to reduce E-cadherin transcription in a Notch pathway-dependent manner. In accordance, the number of HCT15 E-cadherin+ cells is significantly reduced when these are cocultured *in vitro* with tumor GFP$^+$Jag2$^+$ (Fig. 3C). This phenotype is reversed upon the addition of GSI or when HCT15 cells are cocultured with GFP$^+$ Jag2 negative cells (Fig. 3E). Taking together these results suggest that bone marrow–derived cells modulate EMT via Jag2 mediated Notch-pathway activation on tumor cells.

Bone marrow–derived CD11b$^+$Jag2$^+$ cells induce EMT via Jag2-mediated Notch pathway activation

Having shown that bone marrow–derived Jag2$^+$ cells are responsible for tumor cell EMT via Notch pathway activation, next we sought to determine the identity of these cells more precisely. The majority of TGFP+ Jag2$^+$ cells were CD11b$^+$ (85 ± 1.0%), F4/80+ (64.1 ± 0,55%), and Sca-1+ (52.5 ± 1.55%) (Fig. 4A, B, and C). Considering the high frequency of CD11b$^+$ cells within the TGFP+ Jag2$^+$ population, we tested whether tumor-derived CD11b$^+$ Jag2$^+$ cells (CD11b$^+$Jag2$^+$) could induce HCT15 EMT *in vitro*. Accordingly, coculture of HCT15 tumor cells with tumor-derived CD11b$^+$Jag2$^+$ cells led to a significant decrease in E-cadherin expression at both the mRNA and

Published OnlineFirst May 30, 2013; DOI: 10.1158/0008-5472.CAN-13-0085

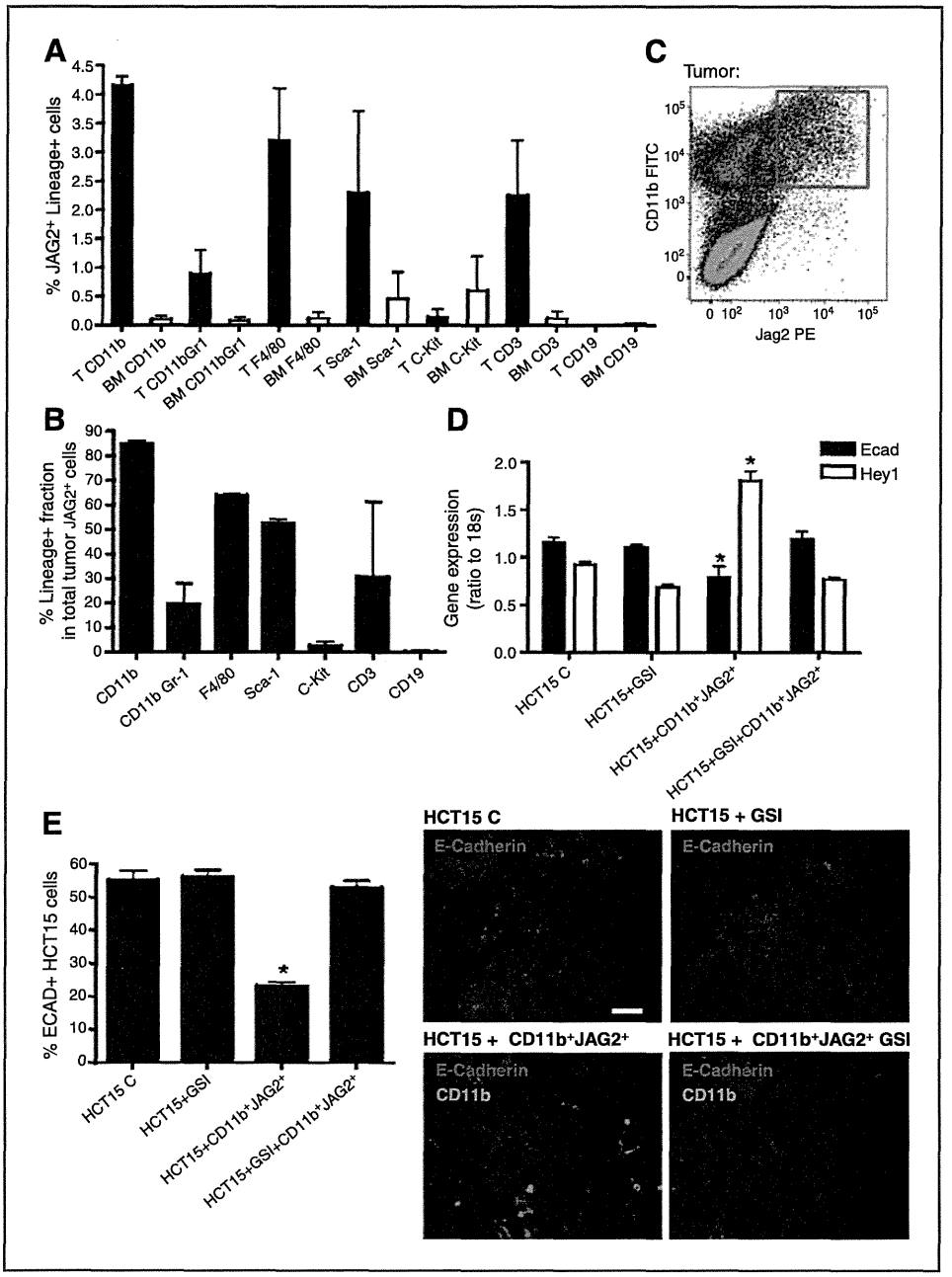

Figure 4. Bone marrow–derived CD11b$^+$Jag2$^+$ cells induce EMT via Jag2–mediated Notch pathway activation. A, quantification of Jag2$^+$ CD11b$^+$/CD11b$^+$ Gr-1+/F4/80+/Sca-1+/c-Kit+/CD3+/CD19+ expressing cells in tumors and corresponding bone marrow samples. B, quantification of the percentage of tumor-infiltrating Jag2$^+$ cells that express CD11b/CD11b Gr-1/F4/80/Sca-1/c-Kit/CD3 or CD19 marker. C, representative flow cytometry plot showing CD11b$^+$Jag2$^+$ BM-derived cells. D, quantification of E-cadherin and Hey 1 gene expression (normalized to 18s rRNA expression) by qRT-PCR on HCT15 alone (HCT15 C), in the presence of 10uM GSI (HCT15 + GSI), in the presence of bone marrow–derived CD11b$^+$Jag2$^+$ cells isolated from tumors (HCT15 + CD11b$^+$Jag2$^+$), and in the presence of 10 μmol/L GSI and tumor associated bone marrow–derived CD11b$^+$Jag2$^+$ cells (HCT15 + CD11b$^+$Jag2$^+$ + GSI). E, quantification of E-cadherin+ on HCT15 C, HCT15 + GSI, HCT15 + CD11b$^+$Jag2$^+$, and HCT15 + CD11b$^+$Jag2$^+$ + GSI groups. Representative images of E-cadherin (red) expression in HCT15 cells and CD11b (green) expression on tumor associated CD11b$^+$ Jag2$^+$ cells. Panel shows representative pictures of coculture experiments where E-cadherin is labeled in red and CD11b bone marrow–derived cells are labeled in green. Scale bar, 50 μm. Data shown are means ± SEM of 3 independent experiments ($n = 3$), *, $P < 0.05$.

protein level (Fig. 4D and E), in a Notch pathway-dependent manner, as GSI treatment reverted this effect. Altogether these data suggest that CD11b$^+$Jag2$^+$ bone marrow–derived cells actively infiltrate colorectal cancer tumors and induce EMT on tumor cells in a Notch pathway-dependent manner.

CD11b$^+$Jag2$^+$ cells are mobilized to PB and home to tumor tissues in different colorectal cancer models

Considering the observed effect of bone marrow–derived CD11b$^+$Jag2$^+$ cell population in inducing EMT in HCT15 cells *in vitro* and *in vivo*, next we quantified the recruitment of this population in other colon cancer models. For this purpose, we developed subcutaneous colon carcinoma xenotransplants using 3 human colorectal cancer cell lines, HCT15, DLD-1, and HT-29, and evaluated the presence of CD11b$^+$Jag2$^+$ cells in the peripheral blood and in the tumor tissues. There was a significant increase in the frequency of CD11b$^+$Jag2$^+$ cells in the peripheral blood compared with control mice (no tumor) in all models (Fig. 5A), this being particularly evident on HCT15-xenotransplanted mice, which showed a significant increase on days 7 and 14 after tumor inoculation. Moreover, FACS analysis of tumor samples showed that CD11b$^+$Jag2$^+$ cells are present in tumor xenotransplants derived from all cell lines at a frequency ranging from 4.5%–8.5% of total cells (Fig. 5B and C). To further validate the biologic significance of CD11b$^+$Jag2$^+$ cells in

Published OnlineFirst May 30, 2013; DOI: 10.1158/0008-5472.CAN-13-0085

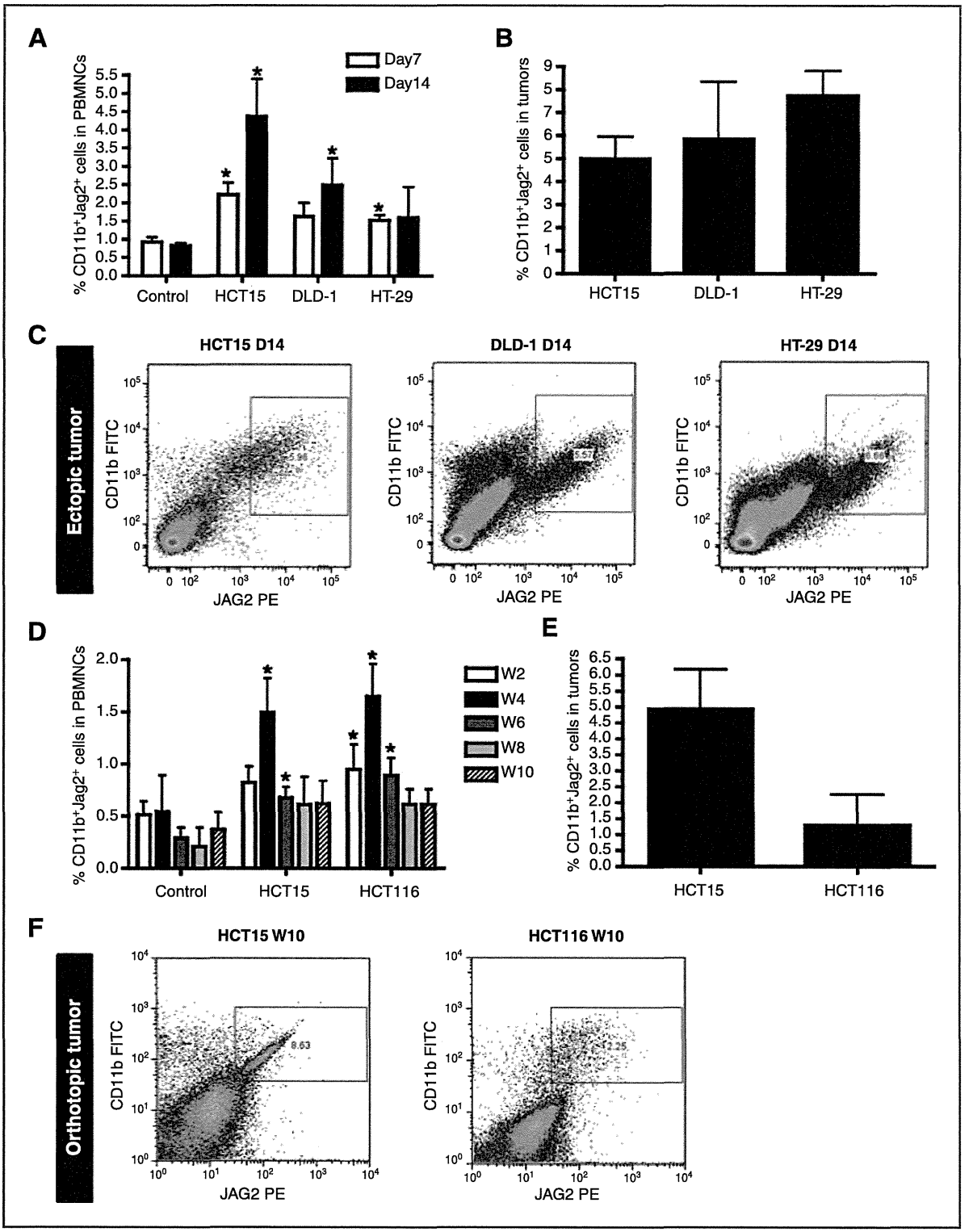

Figure 5. $CD11b^+Jag2^+$ cells are mobilized to PB and home to tumor tissues in different colorectal cancer models. A, flow cytometry–based quantification of $CD11b^+Jag2^+$ percentage in PBMC fraction of control (no tumor) and tumor-bearing mice xenotransplanted with HCT15, DLD-1, and HT-29 colorectal cell lines, 7 and 14 days after ectopic tumor inoculation. B, quantification of $CD11b^+Jag2^+$ percentage in ectopic HCT15, DLD-1, and HT-29 tumor samples. C, representative flow cytometry plot showing $CD11b^+Jag2^+$ cells in ectopic HCT15, DLD-1, and HT-29 tumor samples. D, quantification of $CD11b^+Jag2^+$ percentage in peripheral blood mononuclear cells' (PBMC) fraction of control and tumor-bearing mice xenotransplanted with HCT15 and HCT116 colorectal cell lines at week 2 to 10 after orthotopic tumor inoculation. E, quantification of $CD11b^+Jag2^+$ percentage in orthotopic HCT15 and HCT116 tumor samples. F, representative flow cytometry plot showing $CD11b^+Jag2^+$ cells in orthotopic HCT15 and HCT116 tumor samples. Data are means ± SEM; *, $P < 0.05$; $n = 12$ (3 mice per group in ectopic models) and $n = 12$ (4 mice per group in orthotopic models).

Published OnlineFirst May 30, 2013; DOI: 10.1158/0008-5472.CAN-13-0085

colorectal cancer growth, we developed orthotopic models of colorectal cancer using HCT15 and HCT116 cell lines and evaluated their presence in the peripheral blood and in tumor tissues, as above. Mice bearing orthotopic HCT15 and HCT116 tumors showed increased frequency of peripheral blood $CD11b^+Jag2^+$ cells compared with control mice on weeks 4 and 6, after tumor inoculation (Fig. 5D). Moreover, FACS analysis of tumor samples shows that $CD11b^+Jag2^+$ cells are present in orthotopic tumors at a frequency ranging from 0.5% to 6% of total tumor cells (Fig. 5E and F). Together, these data show that in different murine models of colorectal cancer, $CD11b^+Jag2^+$ cells are mobilized to the peripheral blood and are actively recruited into tumors, which is suggestive of the biologic significance of this population in colorectal cancer growth and EMT onset.

CD11b-neutralizing antibodies reduce $CD11b^+Jag2^+$ cell recruitment, resulting in decreased tumor growth and EMT *in vivo*

To further test the role of $CD11b^+Jag2^+$ in colorectal cancer progression and EMT, we treated mice bearing ectopic HCT15 tumors with neutralizing monoclonal antibodies against CD11b. CD11b neutralization caused a significant reduction in tumor growth (Fig. 6A) and also on the peripheral blood levels of $CD11b^+$ and $CD11b^+Jag2^+$ cells compared with mice treated with vehicle alone (Fig. 6B). Moreover, flow cytometry and immunostaining-based quantification of $CD11b^+$ and $CD11b^+Jag2^+$ cells in tumor tissues showed that CD11b neutralization led to a significant reduction in both cell populations (Fig. 6C–E). Having shown that CD11b neutralization leads to a significant reduction in the number of peripheral blood and tumor-infiltrating $CD11b^+Jag2^+$ cells, we determined its effect in the onset of EMT. As shown in Fig 6, while control (untreated) mice show the expected decrease in E-cadherin expression (Fig. 6F and G), this is sustained and even slightly increases in tumors of mice treated with CD11b-neutralizing antibody. Analysis of Notch pathway downstream targets Hey 1 and Hes 1 expression showed the reduced EMT onset in tumors treated with anti-CD11b–neutralizing antibody is accompanied by decreased activation of the Notch pathway (Fig. 6F), which is in accordance with our *in vitro* data. Taken together, these data suggest that treatment of ectopic colon cancer-bearing mice with neutralizing monoclonal antibodies against CD11b reduces infiltration of $CD11b^+Jag2^+$ cells into the tumors, reducing EMT and reducing Notch pathway activation.

$CD11b^+Jag2^+$ PB and tumor levels correlate with lower E-cadherin expression and metastatic disease in patients with colorectal cancer

Having shown the importance of bone marrow–derived $CD11b^+Jag2^+$ cell population in inducing EMT in murine colorectal cancer models, and the easy quantification of these cells in peripheral blood of colon cancer-bearing mice, next we tested the feasibility and usefulness of quantifying these cells in the samples of patient with colorectal cancer. We quantified the levels of $CD11b^+Jag2^+$ cells in peripheral blood samples of 40 patients with colorectal cancer diagnosed at different stages (according to the AJCC Staging System). For the analysis, patients were classified as: TxN0M0 (patients with colorectal cancer without lymph node or distant metastasis, stages I–II of the AJCC), TxNxM0 (patients with colorectal cancer with lymph node metastasis and without distant metastasis, stage III of the AJCC), and TxNxMx (patients with colorectal cancer with distant metastasis, stage IV of the AJCC). We observed a significant correlation between PB $CD11b^+Jag2^+$ cell levels and colorectal cancer stages, with higher stage colorectal cancer patients showing higher peripheral blood $CD11b^+Jag2^+$ levels (Fig. 7A and B). Moreover, there was an inverse correlation ($P = 0.0197$; $R^2 = 0.4708$, 11 patients) between peripheral blood $CD11b^+Jag2^+$ cell levels and tumor E-cadherin expression (Fig. 7C). We were also able to investigate the relation between $CD11b^+Jag2^+$ tumor levels and colorectal cancer staging in 12 patients. We observed that TxNxM0 and TxNxMx stage patients had significantly higher numbers of $CD11b^+Jag2^+$ cells in tumor samples relatively to TxN0M0 patients (Fig. 7D and E). We also observed a strong inverse correlation ($P = 0.0007$; $R^2 = 0.7011$, 12 patients) between $CD11b^+Jag2^+$ numbers in tumors and tumor E-cadherin expression levels (Fig. 7F). Importantly, in our patient cohort, there was no correlation between tumor size and the presence of peripheral blood or tumor $CD11b^+Jag2^+$ cells (Supplementary Fig. S2). Together, these data strongly suggest that quantification of both $CD11b^+Jag2^+$ cells in the PB and in the tumor samples of patients with colorectal cancer correlates with colorectal cancer staging, and thus may be used as a prognostic or diagnostic marker. These data also validate our data obtained from colorectal cancer mouse models, where we showed $CD11b^+Jag2^+$ cells infiltrate colorectal cancer tumors and induce EMT.

Discussion

Over the last decade, there has been an increase in our understanding of the contribution of tumor stromal components in the regulation of tumor progression and metastasis formation (17). EMT has been shown to be essential for carcinoma progression, namely in breast, colon, and prostate carcinoma, preceding invasion and metastasis formation (3, 18). One of the major molecular regulators of EMT is E-cadherin. E-cadherin is a member of the cadherin family of homophilic cell adhesion molecules and is essential for the maintenance of adherens junctions that confer physical integrity and polarization to epithelial cells. Targeted disruption of E-cadherin during tumor progression resulting in decreased intercellular adhesiveness is one of the most common alterations in human cancers (19, 20). In fact, E-cadherin functional inactivation represents a critical step in the acquisition of invasive capacity by epithelial tumor cells. Accordingly, abolishing E-cadherin function *in vitro* confers invasive properties to noninvasive cells and conversely, introduction of E-cadherin into invasive epithelial cell lines abrogates their invasive potential. Not surprisingly, then, loss of E-cadherin expression is a defining feature of EMT (9). Although many molecular regulators of EMT have been identified, the cellular interactions between tumor cells and tumor stromal cells responsible for tumor EMT are still unclear.

Published OnlineFirst May 30, 2013; DOI: 10.1158/0008-5472.CAN-13-0085

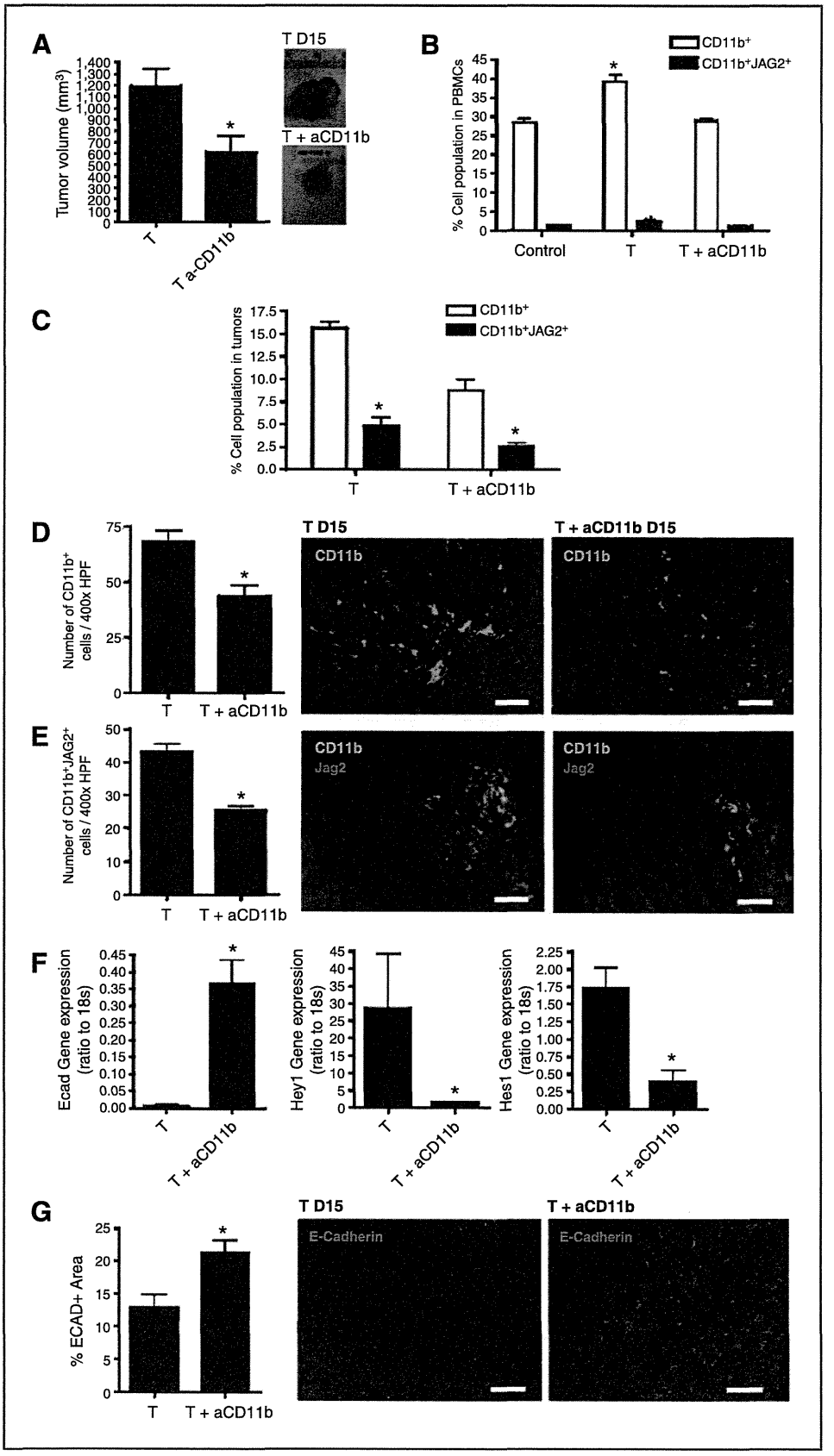

Figure 6. CD11b-neutralizing antibodies *in vivo* administration reduces CD11b$^+$Jag2$^+$ cell recruitment, resulting in decreased tumor growth and EMT. A, ectopic tumor volume quantification in PBS (T) or anti-CD11b (T + a-CD11b)–treated mice, 15 days after inoculation. Representative image of tumors collected at day 15 from control and anti-CD11b–treated mice. B, flow cytometry–based quantification of the percentage of CD11b$^+$ and CD11b$^+$ Jag2$^+$ cells in the mononuclear cell fraction of peripheral blood samples of control (no tumor), PBS (T), and anti-CD11b (T + a-CD11b)–treated mice, 15 days after inoculation. C, flow cytometry–based quantification of the percentage of CD11b$^+$ and CD11b$^+$ Jag2$^+$ cells in tumor samples of PBS (T) and anti-CD11b (T + a-CD11b)–treated mice, 15 days after inoculation. D, immunohistologic quantification of CD11b$^+$ cells in tumor samples of PBS (T) and anti-CD11b (T + a-CD11b)–treated mice per ×400HPF, 15 days after inoculation. Representative images of CD11b$^+$ cells (green) in T and T + aCD11b–treated mice tumor samples. Scale bar, 50 μm. E, immunohistologic quantification of CD11b$^+$ Jag2$^+$ cells in tumor samples of PBS (T) and anti-CD11b (T + a-CD11b)–treated mice per ×400 HPF, 15 days after inoculation. Representative images of CD11b$^+$ (green) Jag2$^+$ (red) cells in T and T + aCD11b treated mice tumor samples. Scale bar, 50 μm. F, quantification of E-cadherin, Hey 1, and Hes 1 gene expression (normalized to 18s rRNA expression) by qRT-PCR in tumor samples of PBS (T) and anti-CD11b (T + a-CD11b)–treated mice. G, quantification of the E-cadherin area percentage in tumor samples of PBS (T) and anti-CD11b (T + a-CD11b)–treated mice. Representative images of E-cadherin+ cells (red) in T and T + aCD11b–treated mice tumor samples. Scale bar, 100 μm. Data are means ± SEM; *, $P < 0.05$; $n = 12$ (4 mice per group: control, T, and T + a CD11b).

Published OnlineFirst May 30, 2013; DOI: 10.1158/0008-5472.CAN-13-0085

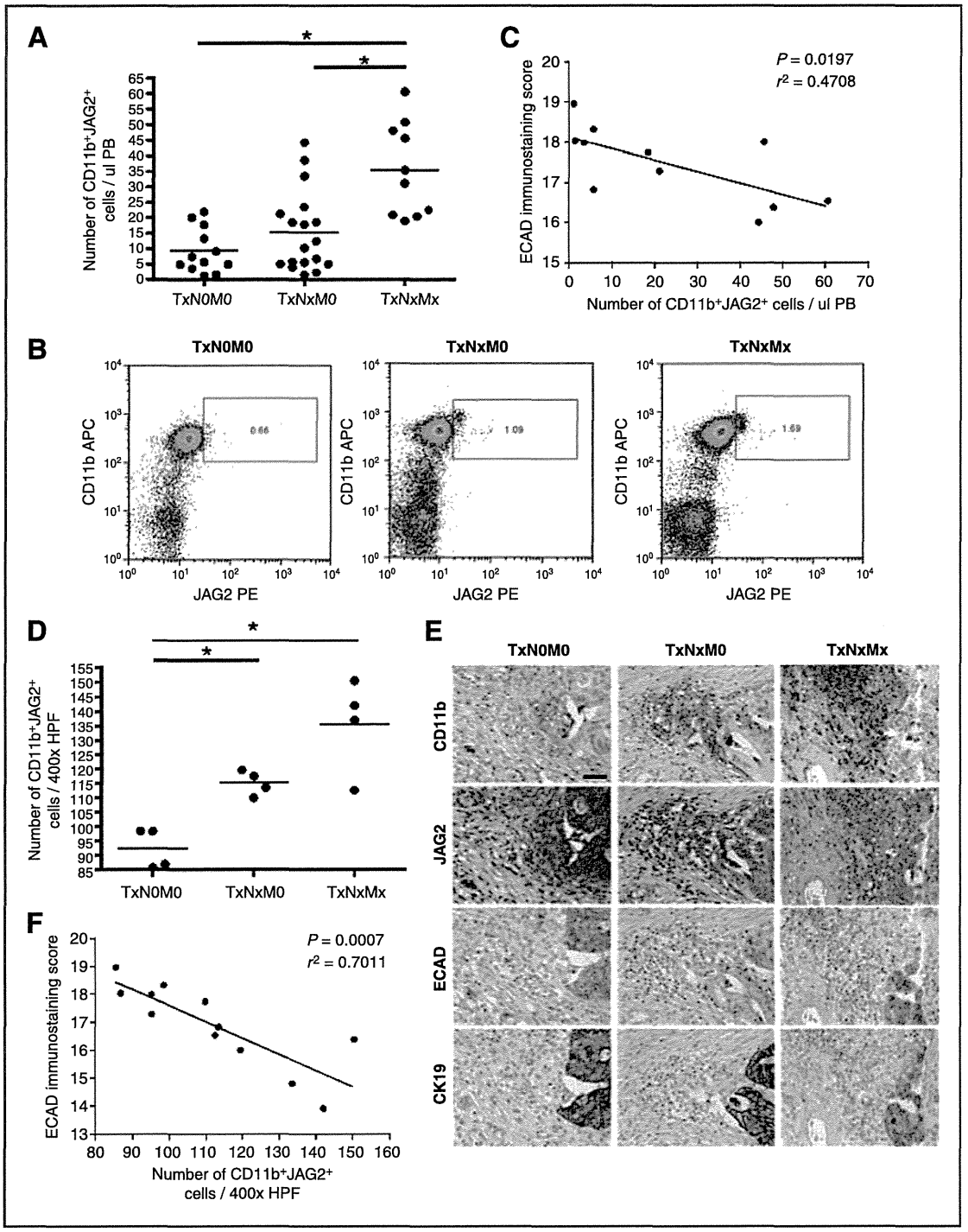

Figure 7. $CD11b^+Jag2^+$ PB and tumor levels correlate with lower E-cadherin expression and metastatic disease in patients with colorectal cancer. A, quantification of the number of $CD11b^+JAG2^+$ cells per μL of peripheral blood samples of patients with colorectal cancer at different stages: TxN0M0 (patients without colorectal cancer lymph node or distant metastasis, stages I-II of the AJCC), TxNxM0 (patients with colorectal cancer lymph node metastasis and without distant metastasis, stage III of the AJCC), and TxNxMx (patients with colorectal cancer distant metastasis, stage IV of the AJCC). B, representative flow cytometry plot showing $CD11b^+$ $Jag2^+$ cells in PB samples of patients with colorectal cancer at different stages. C, correlation plot between the number of $CD11b^+JAG2^+$ cells in circulation and the E-cadherin score determined by immunostaining of primary tumor sections in individual patients with colorectal cancer. D, immunostaining quantification of $CD11b^+JAG2^+$ cells per 400x HPF in primary tumor samples of patients with colorectal cancer at different stages. E, representative images of CD11b, Jag2, E-cadherin, and CK19 (CK-19) immunostainings in serial sections of primary tumor samples of patients with colorectal cancer at different stages. F, correlation plot between the number of tumor $CD11b^+JAG2^+$ cell number per ×400 HPF and the E-cadherin score determined by immunostaining of primary tumor sections in individual patient with colorectal cancer. Data are indicated as means; *, $P < 0.05$ using Mann–Whitney test. Scale bar, 50 μm.

Published OnlineFirst May 30, 2013; DOI: 10.1158/0008-5472.CAN-13-0085

Bone marrow–derived cells, have been shown to directly impact tumor pathophysiology regulating multiple aspects of the metastasization process by modulating tumor angiogenesis, promoting tumor cell invasion, extravasation, intravasation, and micrometastasis establishment, and growth and vascularization (21). However, a role for bone marrow–derived cells in the first steps of metastases formation, namely in EMT, had not been addressed and was the subject of this study. In detail, we investigated a putative role for bone marrow–derived cells in regulating EMT in metastatic colorectal cancer. We show in several ectopic and orthotopic colorectal cancer models that tumor progression is associated with an increased accumulation of bone marrow–derived cells, mainly of myeloid origin. Furthermore, we observe that in late tumors there are regions highly infiltrated by bone marrow–derived cells that show evidence for EMT, namely a robust decrease in E-cadherin expression and a significant increase in vimentin expression in CK19+ tumor cells. It was highly suggestive from our analysis of serial tumor slides that tumor cells (CK19+) in close proximity with bone marrow–derived cells (GFP^+) showed the described hallmarks of EMT. This observation led us to speculate that a direct interaction between bone marrow–derived and tumor cells could modulate EMT in the latter. To test this hypothesis, we used *in vitro* coculture systems, where colorectal cancer cell lines are cultured with bone marrow–derived tumor stromal cells (GFP^+). We used this simple system to investigate the molecular regulation of EMT induction by bone marrow–derived tumor-associated cells. Although TGF-β pathway activation has been extensively described as an inducer of EMT (22), inhibition of TGF-β with neutralizing antibodies in our coculture experiments failed to inhibit the EMT-inducing capacity of bone marrow–derived cells. On the other hand, the Notch pathway has also been associated with EMT and metastasis formation in pancreatic (23) and colorectal cancer (24). Moreover, Notch pathway activation was shown in breast cancer brain metastasis (25). Another study shows that in patients with breast cancer, increased expression of either Jag1 or Notch1 is predictive of poor overall survival (26). Moreover, in colon cancer, Notch 1 overexpression has been shown to correlate with pathologic grade, progression, and metastasis (27). Considering this, we tested the effect of GSI (Notch pathway inhibitor) in reversing the EMT induction by bone marrow–derived cells on colorectal cancer cell lines. GSI addition inhibited EMT induction by bone marrow–derived cells, accompanied by a significant reduction in the expression of Notch pathway downstream targets Hey 1 and 2. Although we did not address Notch downstream effectors regulating EMT, recent studies suggest the mechanisms by which Notch may induce EMT might involve activation of E-cadherin transcriptional repressor Snail2 (28, 29).

Importantly, we show that the bone marrow–derived tumor-infiltrating cells, which are mainly of myeloid origin ($CD11b^+$), increased expression of Jag2, but not of other Notch ligands. Interestingly, Jag2 expression in tumor cells has been recently described as a major regulator of EMT and metastases in lung adenocarcinoma via a miR-200–dependent downstream mechanism (30). Furthermore, quantification of the GFP^+ $Jag2^+$ populations present in the bone marrow and in the tumors revealed a 10-fold increase in the percentage of this population in tumors, suggesting that bone marrow–derived $Jag2^+$ cells are actively recruited into tumors. The signal(s) responsible for the selective recruitment of this specific bone marrow–derived cell population into colon tumors remain undisclosed; we measured the most commonly studied chemokines including SDF1α, MCP1, but these were not actively secreted in our colon cancer models (data not shown). Moreover, recent studies also showed that microparticles/microvesicles/exosomes released by tumors may communicate and "educate" the bone marrow microenvironment, resulting in selective recruitment of bone marrow–derived cells to sites of metastases to form the premetastatic niche (31). Whether specific colon cancer-derived exosomes selectively induce the mobilization of $CD11b^+Jag2^+$ cells is undisclosed. Concerning the molecular mechanisms regulating Jag2 expression, recent data indicate its expression on breast cancer cells is regulated by hypoxia and is directly involved in breast cancer metastases (32). It is therefore legitimate to speculate that during colorectal cancer growth, recruited bone marrow–derived $CD11b^+$ cells enter the tumor site and are exposed to signals from the tumor microenvironment including hypoxia that regulate the expression of Jag2. As shown here, once the infiltrating cells express Jag2, these are capable of inducing EMT on subsets of colon cancer cells. The relative contribution of Jag2 expressed by infiltrating bone marrow–derived cells and by tumor cells proper for the onset of EMT is still undisclosed and will be the subject of future studies in our laboratory.

These findings led us to hypothesize that selective targeting of the $CD11b^+Jag2^+$ bone marrow–derived population might delay the onset of EMT, a first step in the metastasis cascade. As we do not presently have access to specific monoclonal-neutralizing antibodies to Jag2, we sought to impede the recruitment of $CD11b^+$ cells (which include the $Jag2^+$ population) into the tumors. Several studies followed a similar approach and concluded that targeting the $CD11b^+$ population of infiltrating cells may be of therapeutic benefit (33, 34). Moreover, Toh and colleagues (35) recently showed myeloid-derived suppressor cells (also $CD11b^+$) promote EMT, although they did not identify the mechanism involved. In our colon cancer models, CD11b neutralization led to a significant decrease in $CD11b^+Jag2^+$ cell levels in peripheral blood and tumor, delayed EMT, and reduced Notch pathway activation in the tumors. Together, these data strongly suggest that bone marrow–derived $CD11b^+Jag2^+$ cells represent a targetable cell population, which is actively recruited into tumors and induces EMT in a Notch pathway-dependent manner.

Having shown the biologic significance of $CD11b^+Jag2^+$ cells in mouse models of colorectal cancer, we investigated the involvement of this cell population in human colorectal cancer progression. We observed that peripheral blood levels of $CD11b^+Jag2^+$ cells correlate with colorectal cancer stages, with higher levels of $CD11b^+Jag2^+$ cells being observed in

Published OnlineFirst May 30, 2013; DOI: 10.1158/0008-5472.CAN-13-0085

colorectal cancer patients with metastatic disease (mostly consisting of liver metastases), whereas lower $CD11b^+Jag2^+$ levels are detected in patients with colorectal cancer without metastatic disease. Furthermore, we found a significant correlation between $CD11b^+Jag2^+$ cell peripheral blood levels and the levels of E-cadherin expression in the corresponding (i.e., patient-specific) tumor tissues. Taking this into account, we suggest the $CD11b^+Jag2^+$ cells are biologically relevant in human colorectal cancer and that measuring the peripheral blood levels of $CD11b^+Jag2^+$ cells in patients with colorectal cancer may be used as a biomarker to support colorectal cancer staging.

Our data highlight the importance of looking at the initial steps of the metastasis cascade also in a systemic manner. In detail, we show a bone marrow–derived $CD11b^+Jag2^+$ population can activate Notch signaling on colon cancer cells, resulting in EMT induction *in vitro* and *in vivo*. Given the recent excitement from clinical trials using Notch pathway inhibitors for the treatment of tumors, and particularly aiming at blocking tumor angiogenesis (36, 37), the data presented here paves the way for the use of Notch pathway inhibitors to impede metastases onset, by impeding EMT induction at a primary tumor site.

Disclosure of Potential Conflicts of Interest

No potential conflicts of interest were declared.

Authors' Contributions

Conception and design: F. Caiado, I. Rosa, H. Yagita, P. Fidalgo, A.D. Pereira, S. Dias

Development of methodology: F. Caiado, T. Carvalho, H. Yagita

Acquisition of data (provided animals, acquired and managed patients, provided facilities, etc.): F. Caiado, I. Rosa, A. Costa, B. Heissig, K. Hattori, J.P. da Silva, P. Fidalgo

Analysis and interpretation of data (e.g., statistical analysis, biostatistics, computational analysis): F. Caiado, A. Costa, P. Fidalgo, A.D. Pereira, Sérgio Dias

Writing, review, and/or revision of the manuscript: F. Caiado, I. Rosa, H. Yagita, P. Fidalgo, A.D. Pereira, S. Dias

Administrative, technical, or material support (i.e., reporting or organizing data, constructing databases): F. Caiado, L. Remedio, J. Matos

Study supervision: H. Yagita, A.D. Pereira, S. Dias

Acknowledgments

The authors thank the members of the Angiogenesis Lab for their input and suggestions.

Grant Support

This study was supported by Fundaçao para a Ciencia e Tecnologia (FCT, Portuguese Government) grants (S. Dias) and fellowships.

The costs of publication of this article were defrayed in part by the payment of page charges. This article must therefore be hereby marked advertisement in accordance with 18 U.S.C. Section 1734 solely to indicate this fact.

Received January 17, 2013; revised April 3, 2013; accepted April 18, 2013; published OnlineFirst May 30, 2013.

References

1. Chambers AF, Groom AC, MacDonald IC. Metastasis: dissemination and growth of cancer cells in metastatic sites. Nat Rev Cancer 2002;2:563–72.
2. Fidler IJ. The pathogenesis of cancer metastasis: the "seed and soil" hypothesis revisited. Nat Rev Cancer 2003;3:453–8.
3. Hugo H, Ackland ML, Blick T, Lawrence MG, Clements JA, Williams ED, et al. Epithelial–mesenchymal and mesenchymal–epithelial transitions in carcinoma progression. J Cell Physiol 2007;213:374–83.
4. Levayer R, Lecuit T. Breaking down EMT. Nat Cell Biol 2008;10:757–9.
5. Sommers CL, Heckford SE, Skerker JM, Worland P, Torri JA, Thompson EW, et al. Loss of epithelial markers and acquisition of vimentin expression in adriamycin- and vinblastine-resistant human breast cancer cell lines. Cancer Res 1992;52:5190–7.
6. Hay ED, Zuk A. Transformations between epithelium and mesenchyme: normal, pathological, and experimentally induced. Am J Kidney Dis 1995;26:678–90.
7. Radisky DC. Epithelial–mesenchymal transition. J Cell Sci 2005;118:4325–6.
8. Kalluri R, Weinberg RA. The basics of epithelial–mesenchymal transition. J Clin Invest 2009;119:1420–8.
9. Bates RC, Mercurio AM. The epithelial–mesenchymal transition (EMT) and colorectal cancer progression. Cancer Biol Ther 2005;4:365–70.
10. Iwatsuki M, Mimori K, Yokobori T, Ishi H, Beppu T, Nakamori S, et al. Epithelial–mesenchymal transition in cancer development and its clinical significance. Cancer Sci 2010;101:293–9.
11. Joyce JA, Pollard JW. Microenvironmental regulation of metastasis. Nat Rev Cancer 2009;9:239–52.
12. Pollard JW. Tumour-educated macrophages promote tumour progression and metastasis. Nat Rev Cancer 2004;4:71–8.
13. Condeelis J, Pollard JW. Macrophages: obligate partners for tumor cell migration, invasion, and metastasis. Cell 2006;124:263–6.
14. Kaplan RN, Riba RD, Zacharoulis S, Bramley AH, Vincent L, Costa C, et al. VEGFR1-positive haematopoietic bone marrow progenitors initiate the pre-metastatic niche. Nature 2005;438:820–7.
15. Gao D, Nolan DJ, Mellick AS, Bambino K, McDonnell K, Mittal V. Endothelial progenitor cells control the angiogenic switch in mouse lung metastasis. Science 2008;319:195–8.
16. ImmunoMembrane. Available from: http://imtmicroscope.uta.fi/immunomembrane/≥.
17. Albini A, Sporn MB. The tumour microenvironment as a target for chemoprevention. Nat Rev Cancer 2007;7:139–47.
18. Arias AM. Epithelial–mesenchymal interactions in cancer and development. Cell 2001;105:425–31.
19. Hirohashi S. Inactivation of the E-cadherin-mediated cell adhesion system in human cancers. Am J Pathol 1998;153:333–9.
20. Hanahan D, Weinberg RA. The hallmarks of cancer. Cell 2000;100:57–70.
21. Gao D, Mittal V. The role of bone-marrow-derived cells in tumor growth, metastasis initiation and progression. Trends Mol Med 2009;15:333–43.
22. Thiery JP, Acloque H, Huang RYJ, Nieto MA. Epithelial–mesenchymal transitions in development and disease. Cell 2009;139:871–90.
23. Kang M, Jiang B, Xu B, Lu W, Guo Q, Xie Q, et al. Delta like ligand 4 induces impaired chemo-drug delivery and enhanced chemoresistance in pancreatic cancer. Cancer Lett 2013;330:11–21.
24. Sureban SM, May R, Mondalek FG, Qu D, Ponnurangam S, Pantazis P, et al. Nanoparticle-based delivery of siDCAMKL-1 increases microRNA-144 and inhibits colorectal cancer tumor growth via a Notch-1 dependent mechanism. J Nanobiotechnol 2011;9:40.
25. Nam DH, Jeon HM, Kim S, Kim MH, Lee YJ, Lee MS, et al. Activation of Notch signaling in a xenograft model of brain metastasis. Clin Cancer Res 2008;14:4059–66.
26. Reedijk M, Odorcic S, Chang L, Zhang H, Miller N, McCready DR, et al. High-level coexpression of JAG1 and NOTCH1 is observed in human breast cancer and is associated with poor overall survival. Cancer Res 2005;65:8530–7.

Published OnlineFirst May 30, 2013; DOI: 10.1158/0008-5472.CAN-13-0085

27. Zhang Y, Li B, Ji ZZ, Zheng PS. Notch 1 regulates the growth of human colon cancers. Cancer 2010;116:5207–18.
28. Leong KG, Niessen K, Kulic I, Raouf A, Eaves C, Pollet I, et al. Jagged1-mediated Notch activation induces epithelial-to-mesenchymal transition through Slug-induced repression of E-cadherin. J Exp Med 2007; 204:2935–48.
29. Wang Z, Li Y, Kong D, Sarkar FH. The role of Notch signaling pathway in epithelial–mesenchymal transition (EMT) during development and tumor aggressiveness. Curr Drug Targets 2010;11: 745–51.
30. Yang Y, Ahn YH, Gibbons DL, Zang Y, Lin W, Thilaganathan N, et al. The Notch ligand Jagged2 promotes lung adenocarcinoma metastasis through a miR-200-dependent pathway in mice. J Clin Invest 2011; 121:1373–85.
31. Peinado H, Aleckovic M, Lavotshkin S, Matei I, Costa-Silva B, Moreno-Bueno G, et al. Melanoma exosomes educate bone marrow progenitor cells toward a pro-metastatic phenotype through MET. Nat Med 2012;18:883–91.
32. Xing F, Okuda H, Watabe M, Kobayashi A, Pai SK, Liu W, et al. Hypoxia-induced Jagged2 promotes breast cancer metastasis and self-renewal of cancer stem-like cells. Oncogene 2011;30: 4075–86.
33. Ishihara M, Nishida C, Tashiro Y, Gritli I, Rosenkvist J, Koizumi M, et al. Plasmin inhibitor reduces T-cell lymphoid tumor growth by suppressing matrix metalloproteinase-9-dependent CD11b(+)/F4/80(+) myeloid cell recruitment. Leukemia 2012;26:332–9.
34. Ahn GO, Tseng D, Liao CH, Dorie MJ, Czechowicz A, Brown JM. Inhibition of Mac-1 (CD11b/CD18) enhances tumor response to radiation by reducing myeloid cell recruitment. Proc Natl Acad Sci U S A 2010;107:8363–8.
35. Toh B, Wang X, Keeble J, Sim WJ, Khoo K, Wong WC, et al. Mesenchymal transition and dissemination of cancer cells is driven by myeloid-derived suppressor cells infiltrating the primary tumor. PLoS Biol 2011;9:e1001162.
36. Thurston G, Noguera-Troise I, Yancopoulos GD. The Delta paradox: DLL4 blockade leads to more tumour vessels but less tumour growth. Nat Rev Cancer 2007;7:327–31.
37. Wang Z, Li Y, Banerjee S, Sarkar FH. Exploitation of the notch signaling pathway as a novel target for cancer therapy. Anticancer Res 2008; 28:3621–30.

PLOS ONE

High Concentrations of L-Ascorbic Acid Specifically Inhibit the Growth of Human Leukemic Cells via Downregulation of *HIF-1α* Transcription

Hiroshi Kawada[1,2*☯], Mitsuyo Kaneko[1,2☯], Masakazu Sawanobori[1], Tomoko Uno[2], Hideyuki Matsuzawa[2], Yoshihiko Nakamura[2], Hiromichi Matsushita[2,3], Kiyoshi Ando[1,2]

1 Division of Hematology/Oncology, Department of Medicine, Tokai University School of Medicine, Isehara, Kanagawa, Japan, **2** Research Center for Regenerative Medicine, Tokai University School of Medicine, Isehara, Kanagawa, Japan, **3** Department of Laboratory Medicine, Tokai University School of Medicine, Isehara, Kanagawa, Japan

Abstract

We examined the antileukemic effects of high concentrations of L-ascorbic acid (high AA) on human leukemic cells. In vitro, high AA markedly induced apoptosis in various leukemic cell lines by generating hydrogen peroxide (H_2O_2) but not in normal hematopoietic stem/progenitor cells. High AA significantly repressed leukemic cell proliferation as well as neoangiogenesis in immunodeficient mice. We then noted that in leukemic cells, *HIF-1α* transcription was strongly suppressed by high AA and correlated with the transcription of *VEGF*. Our data indicate that exposure to high AA markedly increased the intracellular AA content of leukemic cells and inhibited the nuclear translocation of NF-κB, which mediates expression of HIF-1α. We next generated K562 cells that overexpressed *HIF-1α* (K562-HIF1α cells) and assessed the mechanistic relationship between inhibition of *HIF-1α* transcription and the antileukemic effect of high AA. The ability of high AA to induce apoptosis was significantly lower in K562-HIF1α cells than in K562 cells in vitro. We found that expression of HIF-1α-regulated antiapoptotic proteins of the Bcl-2 family, such as Mcl-1, Bcl-x_L, and Bcl-2, was significantly suppressed by high AA in K562 cells, but was sustained at higher levels in K562-HIF1α cells, regardless of high AA exposure. Moreover, repression of cell proliferation and neoangiogenesis by high AA was completely abrogated in mice receiving transplants of K562-HIF1α cells. These results indicate that, along with H_2O_2 generation, downregulation of *HIF-1α* transcription plays a crucial role in growth inhibition of human leukemic cells by high AA.

Citation: Kawada H, Kaneko M, Sawanobori M, Uno T, Matsuzawa H, et al. (2013) High Concentrations of L-Ascorbic Acid Specifically Inhibit the Growth of Human Leukemic Cells via Downregulation of *HIF-1α* Transcription. PLoS ONE 8(4): e62717. doi:10.1371/journal.pone.0062717

Editor: Amina Ann Qutub, Rice University, United States of America

Received July 10, 2012; **Accepted** March 25, 2013; **Published** April 23, 2013

Funding: This work was supported by grants from Tokai University and The Ministry of Education, Culture, Sports, Science, and Technology of Japan (MEXT)-Supported Program for the Strategic Research Foundation at Private Universities. The funders had no role in study design, data collection and analysis, decision to publish, or preparation of the manuscript.

Competing Interests: The authors have declared that no competing interests exist.

* E-mail: hkawada@is.icc.u-tokai.ac.jp

☯ These authors contributed equally to this work.

Introduction

Pauling and Cameron were the first to report that when L-ascorbic acid (AA) was given intravenously to human cancer patients for 10 days and then orally in pharmacologic doses of 10 g daily, it was effective in treating some cancers and in improving patient survival [1,2]. The same oral dose had no therapeutic effects on cancer patients in 2 subsequent double-blind placebo-controlled trials [3,4]. However, we thought that it was important to examine anew the role of AA in cancer treatment for the reasons that follow: (i) the route of AA administration leads to large differences in plasma concentrations, and intravenous administration results in 70-times higher plasma concentration than oral administration [5]; (ii) high concentrations of AA (high AA) administered intravenously exert remarkable anticancer effects by generating hydrogen peroxide (H_2O_2) in the extracellular fluid of tumor-bearing animals [6,7]; and (iii) recent clinical studies also demonstrate the antitumor effects of intravenous high AA in patients with different types of cancers [8,9]. Further, it is remarkable that the cytotoxic effects of high AA appear to be cancer cell-type specific [7].

In the present study, we attempted, therefore, to determine whether high AA exerts significant cytotoxic effects against human leukemic cells in vitro and in vivo. We confirm here that the leukemic cell-specific cytotoxic effects of high AA were caused by the generation of H_2O_2. Further, while HIF-1α plays an important role biologically and clinically in myeloid and lymphoid leukemias [10–15], we found that high AA strongly inhibited HIF-1α expression in leukemic cells.

HIF-1 is composed of an inducible (HIF-1α) and a constitutively expressed subunit (HIF-1β) [16]. HIF-1α contains an oxygen-dependent degradation domain, which when hydroxylated by specific prolyl hydroxylases, binds the von Hippel–Lindau protein, leading to the ubiquitination of HIF-1α and its degradation by the 26S proteasome. At low oxygen levels, the prolyl hydroxylases lose their activity, which prevents hydroxylation and subsequent binding to the von Hippel–Lindau protein [17,18]. This results in HIF-1α stabilization, nuclear translocation, dimerization with

the β-subunit, and binding to recognition elements in the promoters of target genes.

AA facilitates the hydroxylation of HIF-1α via the stimulation of the prolyl hydroxylases [19,20]. However, we have shown here that high AA markedly inhibit the expression of HIF-1α in leukemic cells at the level of transcription. We have further demonstrated that one important mechanism underlying this response is the transcriptional regulation of HIF-1α by the redox-sensitive transcription factor NF-κB, which has been shown to bind at a distinct element in the proximal promoter of *HIF-1α* under not only hypoxic but also non-hypoxic conditions and regulate *HIF-1α* transcription [21]. Most important, the inhibition of HIF-1α expression is considered to play a crucial role in the antileukemic effects of high AA.

Materials and Methods

Cells

The human leukemic cell lines, K562 (blast crisis of chronic myeloid leukemia), HL60 (promyelocytic leukemia), MOLM14 (monocytic leukemia), NB4 (promyelocytic leukemia), Jurkat (T-lymphoblastic leukemia), and Raji (B-lymphoblastic leukemia), were maintained in RPMI 1640 medium supplemented with 10% heat-inactivated fetal bovine serum (FCS) and antibiotics (100 U penicillin/ml and 100 μg streptomycin/ml) at 37°C in a humidified 5% CO_2 atmosphere. The MOLM-14 cell line [22] was kindly provided by the Cell Biology Institute, Research Center, Hayashibara Biochemical Laboratories. The NB4 cell line was purchased from the German Collection of Microorganisms and Cell Cultures. The remaining cell lines were purchased from the American Type Culture Collection. Human umbilical cord blood (CB) samples were harvested from subjects quickly after birth, after written informed consent was obtained in accordance with the Declaration of Helsinki and with approval from the Tokai University Committee on Clinical Investigation. The $CD34^+$ cell fraction was prepared using the CD34 Progenitor Cell Isolation Kit (Miltenyi Biotec) [23]. The CB-$CD34^+$ cells were frozen in a medium supplemented with dimethylsulfoxide and FCS using a step-down freezing procedure and placed in liquid nitrogen. Aliquots of frozen samples were thawed just before use. The thawed cells were washed twice and viability was determined using trypan blue. When cell viability was more than 95%, the samples were subjected to further studies. To prepare K562 cells that overexpressed HIF-1α, we transfected 293T cells with CSII-HIF1α-IRES-EGFP lentiviral vectors for 72 h and collected the supernatant. K562 cells were incubated with the highly concentrated viral supernatant at a multiplicity of infection of 50 for 24 h. Green fluorescent protein-positive K562 cells were then sorted using a FACSVantage cell sorter (Becton Dickinson).

AA

AA was buffered to pH 7.0 with sodium hydroxide and prepared immediately before use.

H_2O_2 assay

AA was added to the medium in 96-well culture plates at the concentrations indicated in the figures. H_2O_2 was quantitated using a Chemiluminescent H_2O_2 Detection Kit (Assay Designs) according to the manufacturer's protocol.

Cell viability assays

AA was added at varying concentrations to 96-well culture plates containing 5×10^3 cells/well. Saline solution was used as a vehicle control. One hour later, cells were washed and resuspended in the culture medium. Seventy-two hours later, the viability of the cells was measured with a nonradioactive cell proliferation assay using the Cell Counting Kit-8 (Dojindo) according to the manufacturer's protocol.

Measurement of apoptosis

Ten thousand cells were incubated with the vehicle, 2800 μM AA, or 2800 μM AA and 600 U/ml of catalase for 1 h and then washed and cultured in the medium. The cells were harvested 18 h later and stained with fluorescein isothiocyanate (FITC)- or allophycocyanin (APC)-labeled annexin V (BD Biosciences) and propidium iodide (PI) (Roche), or with primary anti-cleaved caspase-3 antibody (Cell Signaling) and secondary phycoerythrin (PE)-labeled antibody (eBioscience), according to the manufacturer's instructions. The treated cells were then analyzed using a FACScan flow cytometer (Becton Dickinson).

Measurement of intracellular catalase activity

The intracellular catalase activity of 2×10^4 cells was measured using a Fluorescent Catalase Detection Kit (Fluoro: Catalase™, Cell Technology) according to the manufacturer's instructions. Briefly, the kit utilizes a non-fluorescent substrate, 10-acetyl-3,7-dihydroxyphenoxazine, which is converted by residual H_2O_2 to the fluorescent molecule resorufin.

Histochemical catalase assay

Cell preparations (2×10^5) were placed on glass slides in a cytospin centrifuge and fixed with 4% paraformaldehyde (PFA) for 5 min. The slides were incubated with a rabbit anti-catalase antibody (Sigma Aldrich) overnight at 4°C and then with a horseradish peroxidase-conjugated anti-rabbit antibody (GE Healthcare, Japan) for 4 h at 4°C. After the slides were washed, they were stained with 3,3′-diaminobenzidine tetrahydrochloride, and images were acquired using a digital camera (AxioCam MRc5, Carl Zeiss).

Xenograft and Treatment Procedures

Leukemic cells (2×10^6) were mixed with 100 μl basement membrane matrix (BD Biosciences), and the mixture was transplanted subcutaneously into the right flank of 8-week-old nude mice. On day 8 after transplantation, the tumor volume was measured, and the mice were then injected intravenously with 100 μl of AA at a high concentration (0.5 mg/g body weight, which is similar to the pharmacologic doses for humans and rats [6,7,24–26]), or saline solution as a bolus twice daily for the designated periods. The tumor volume was measured at the times indicated in the figures. All experimental procedures and protocols involving animals were approved by the Animal Care Committee of Tokai University and were in compliance with the ARRIVE guidelines [27].

Immunohistochemical and immunocytochemical analyses

Isoflurane inhalation was used to anesthetize mice, and the tumor was perfused from the apex of the heart with phosphate-buffered saline (PBS) and fixed by perfusion with 4% PFA in PBS. The tumor was then dissected and immersed in 4% PFA overnight at 4°C, embedded in O.C.T. compound (Sakura Finetek, Japan), and then frozen in liquid nitrogen. Cryostat sections (6 μm thick) of the tumor or cytospin specimens of leukemic cells fixed with 4% PFA were stained with specific antibodies and incubated overnight at 4°C. Rat anti-mouse CD31 (BD Sciences) and rabbit anti-NF-κB p65 antibodies (Cell Signaling Technology) were used as

primary antibodies. The slides were then incubated with a secondary antibody conjugated with Alexa488 (Life Technologies). Nuclei were stained with 4′,6-diamidino-2-phenylindole (DAPI; Life Technologies). The slides were observed using a confocal laser-scanning microscope (LSM510 META spectrometer, Carl Zeiss).

Analysis of angiogenesis-related and antiapoptotic molecules

Cells were treated with a high AA (2800 μM). After 1 h, the cells were washed, cultured for 24 h, unless otherwise indicated, and then assayed.

Quantitative real-time polymerase chain reaction

RNA was isolated using the RNeasy Micro Kit (QIAGEN) and reverse transcribed. Each target cDNA was polymerase chain reaction (PCR)-amplified on the same plate by using the TaqMan(R) Gene Expression Assays (Life Technologies Corporation) and the ABI 7300 Real-Time PCR System (Applied Biosystems). The PCR primers used were derived from *HIF-1α* (Applied Biosystems, Assay ID; Hs00936376_m1) and *VEGF* (Applied Biosystems, Assay ID; Hs00900055_m1). The relative amounts of target genes were determined in reference to 18S rRNA. Comparative threshold cycle (C_T) analysis was used to quantify transcripts. The value was calculated by the expression $2^{-\Delta\Delta CT}$.

Western blotting

Cells were harvested and washed, and the pellets were suspended in 0.1 ml of ice-cold TNE buffer and incubated on ice for 10 min. When subcellular fractions were prepared, the Subcellular Proteome Extraction Kit (Calbiochem) was used according to the manufacturer's instructions. The lysates were then centrifuged, and the supernatants were boiled in SDS sample buffer. The proteins were separated on SDS-polyacrylamide gels, electroblotted onto a nitrocellulose membrane, and detected using the ECL Plus Western blotting analysis system (GE Lifesciences) using specific antibodies. Anti-HIF-1α and anti-β-actin antibodies were purchased from BD Biosciences and Sigma-Aldrich, respectively. Anti-p-IκB, anti-NF-κB, anti-Bcl-2, anti-Bcl-x_L, anti-caspase-3, and anti-lamin A/C antibodies were purchased from Cell Signaling Technology. Anti-Mcl-1, anti-Sp1, anti-Sp3, and anti-Sp4 were purchased from Santa Cruz Biotechnology, Inc.

Quantitative assays for intracellular AA content

Cells were treated with 2800 μM AA for 1 h, washed twice in PBS, and then assayed for AA content using a vitamin C assay kit (Shima Laboratories) according to the manufacturer's instructions. Briefly, AA in a given sample is converted by the oxidizing agent to dehydroascorbic acid. Dehydroascorbic acid is then derivatized with 2,4-dinitrophenylhydrazine. Total vitamin C (AA + dehydroascorbic acid) concentration is determined by the specific ultraviolet light (UV) absorption of the 2,4-dinitrophenylhydrazine derivative.

Statistics

All the experimental results have been expressed as the arithmetic mean and standard deviation (SD) values. Student's *t*-test was used to evaluate the statistical significance of the differences between unpaired groups.

Results

Cancer-specific cytotoxic effect of high AA on human hematopoietic cells

We first assessed the effect of high AA on the viability of various human leukemic cell lines as well as on normal hematopoietic stem/progenitor cells in vitro. Addition of 280 and 2800 μM of AA, which are approximately 6 and 60-times higher than the physiological level, produced significant amounts of H_2O_2 after 1 h incubation (34.4±4.1 and 134.0±11.8 μM, respectively) and reduced the viability of all myeloid and lymphoid leukemic cells tested but not that of CB-CD34$^+$ cells (Figure 1A). We further found that high AA induced apoptosis in leukemic cells and that this effect was almost completely abrogated by the addition of catalase (Figure 1B). It is important to note that the leukemic cell lines tested generally possessed lower catalase activities than did normal CB-CD34$^+$ cells (Figures 1C and 1D). Thus, we conclude that the induction of apoptosis by high AA was due to the generation of H_2O_2 and was specifically observed in leukemic cells that expressed relatively lower catalase activities.

Inhibitory effect of high AA on leukemic progression in vivo

We next examined the effect of high AA on the progression of leukemia by using an experimental transplantation model. We mixed HL60 cells and basement membrane matrix (BD Biosciences), transplanted the mixture subcutaneously into the right flank of nude mice, and injected high AA or vehicle intravenously. This procedure enabled a precise assessment of tumor burden over time. There were significant differences in tumor volumes between vehicle- and high AA-treated mice 4 days after the final injection (Figures 2A and 2B). We then killed the mice and found that tumor neoangiogenesis was less evident in high AA-treated mice than in vehicle-treated mice (Figures 2C and 2D).

Inhibitory effect of high AA on HIF-1α expression in leukemic cells

We next determined the expression of angiogenesis-related molecules in CB-CD34$^+$ and leukemic cells in the presence of vehicle or high AA. In CB-CD34$^+$ cells, there was no statistically significant difference in the expression of *HIF-1α* mRNA for the 2 conditions (Figure 3A). In contrast, in HL60 cells, expression of *HIF-1α* mRNA markedly decreased because of high AA (Figure 3A). The expression of HIF-1α in HL60 cells was significantly higher than that in CB-CD34$^+$ cells in the absence of high AA but markedly reduced in the presence of high AA (Figure 3B). Moreover, mRNA expression of *VEGF*, an HIF-1α-regulated gene, also reduced along with that of *HIF-1α* over time after incubation of HL60 cells with high AA (Figure 3C).

We then attempted to determine how *HIF-1α* mRNA expression was inhibited by high AA in leukemic cells. *HIF-1α* is known to be transcriptionally regulated by NF-κB, and AA inhibits phosphorylation of the NF-κB inhibitor (IκB) [28]. Therefore, we tested for the presence of phosphorylated IκB (p-IκB) and found that the p-IκB level in HL60 cells was significantly reduced by the addition of high AA (Figure 4A). These data indicate that high AA markedly inhibited the translocation of NF-κB into the nucleus of HL60 cells, but not CB-CD34$^+$ cells (Figure 4B). We demonstrated further that the intracellular content of AA was much higher in leukemic cells than in normal CB-CD34$^+$ cells after incubation with high AA (Figure 4C). These results suggest that the differences in the intracellular uptake of AA

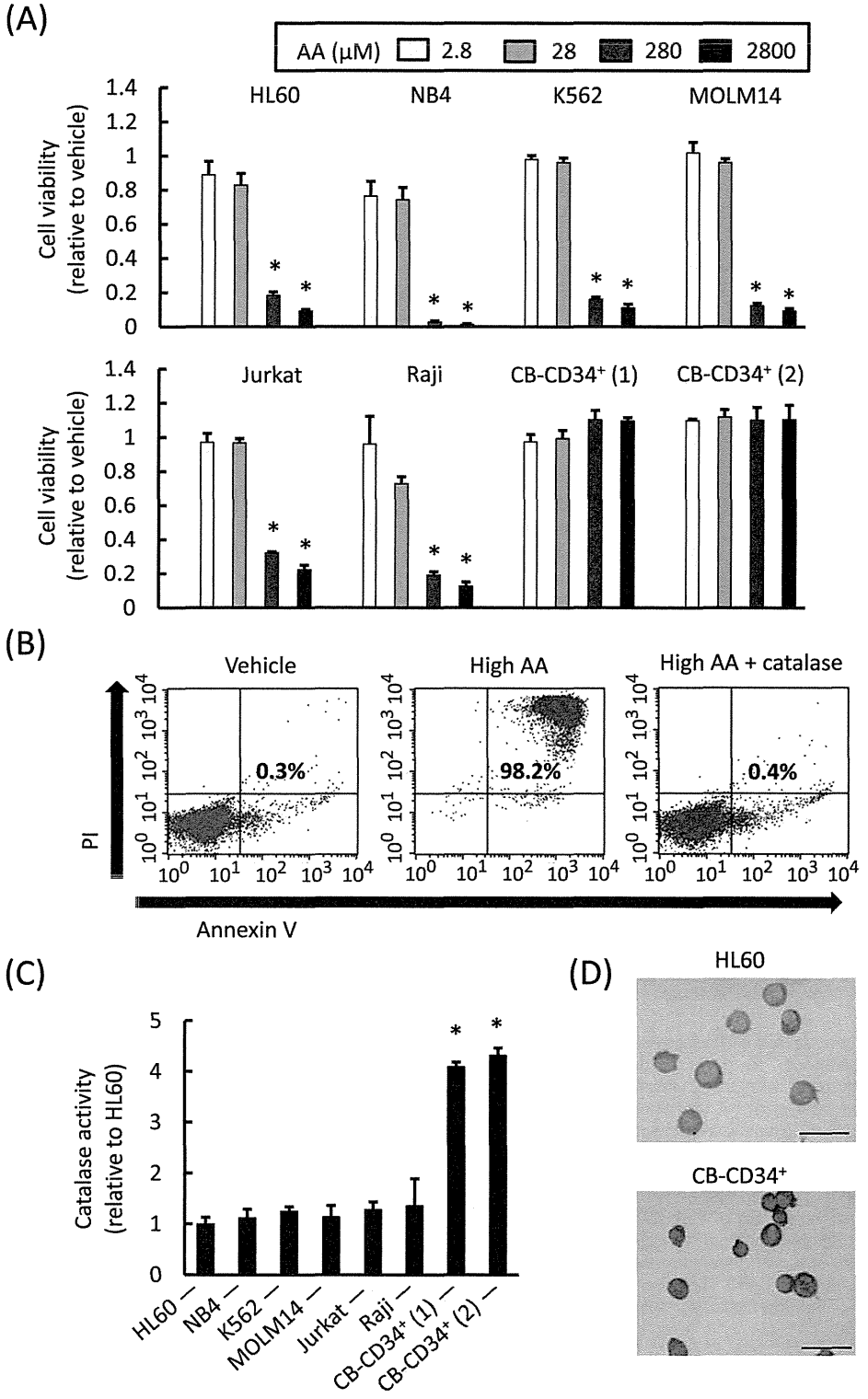

Figure 1. In vitro effects of AA on human leukemic and CB-CD34$^+$ cells, relative to catalase activity. A) Cell viability assay of various leukemic cell lines and 2 independent isolates of CB-CD34$^+$ cells. Cells were treated with different concentrations of AA for 1 h, and then washed, cultured, and analyzed after 72 h. The viability of all cell lines reduced significantly in the presence of 280 and 2800 μM AA (*P<0.0001, as compared with vehicle), but this finding was not obtained for CB-CD34$^+$ cells (P>0.05). The values represent the mean ± SD values of quadruplicate samples. B) Flow cytometric measurement of apoptosis of HL60 cells. Cells were treated with vehicle or AA for 1 h, and then washed, cultured, and analyzed after 18 h. Representative profiles are shown. The annexin V$^+$ propidium iodide (PI)$^+$ cell fraction indicates apoptotic cells. Note that AA-induced apoptosis was almost completely abrogated by the addition of catalase. C) Intracellular catalase activity. Leukemic cells generally expressed lower catalase activities than did CB-CD34$^+$ isolates (*P<0.001, as compared with each cell line). The values represent the mean ± SD values of quadruplicate samples. D) Histochemical analysis demonstrated lower catalase activity in HL60 cells than in CB-CD34$^+$ cells. The bars indicate 50 μm.
doi:10.1371/journal.pone.0062717.g001

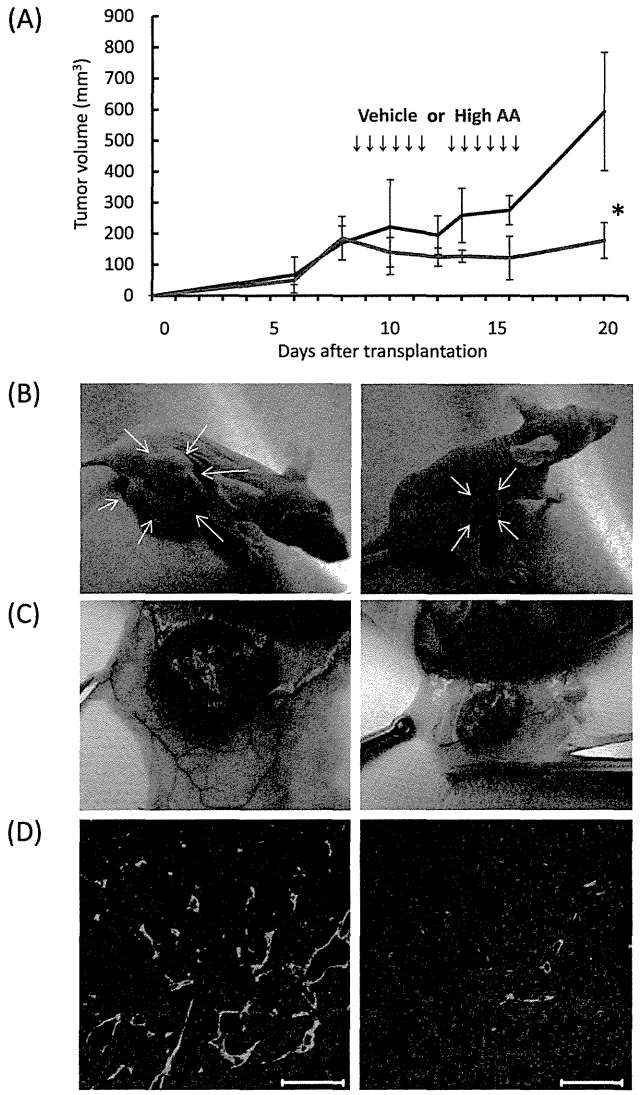

Figure 2. In vivo effects of high AA on progression of leukemia. A) High AA or the vehicle was injected intravenously for 6 days with a rest period of 2 days between 3 daily injections of mice transplanted with HL60 cells. Compared with vehicle (blue line), high AA (red line) significantly inhibited tumor growth (*$P<0.01$). The values represent the mean ± SD values of 5 mice. B) Appearance of mice treated with vehicle (left) and high AA (right), 4 days after the final injection. C) Representative macroscopic appearance of tumors of mice treated with the vehicle (left) and high AA (right). Note that the tumors of high AA-treated mice were smaller and less erythematous than those of vehicle-treated mice. D) Immunohistochemical analysis of tumor neoangiogenesis in mice treated with the vehicle (left) and high AA (right). The green and blue signals represent CD31 and 4′,6-diamidino-2-phenylindole (DAPI), respectively. The bars indicate 100 μm.
doi:10.1371/journal.pone.0062717.g002

reflected the differences seen between high AA-treated human leukemic cells and $CD34^+$ cells derived from normal CB in the presence of NF-κB translocation and following HIF-1α expression.

Relationship between the inhibitory effects of high AA on HIF-1α expression and leukemic progression

Next, we assessed the implications of the inhibition of HIF-1α expression by high AA on leukemic progression by generating *HIF-1α*-overexpressing K562 cells (K562-HIF1α) by using a lentiviral vector. High AA exposure significantly reduced the expression of *HIF-1α* mRNA in K562 but not in K562-HIF1α cells (Figure 5A). The level of HIF-1α in K562-HIF1α cells was also significantly higher than that in K562 cells after vehicle or high AA exposure (Figure 5B). We also found that the induction of apoptosis by high AA was significantly lower in K562-HIF1α than in K562 cells (Figure 5C and 5D). Therefore, we assessed the expression of antiapoptotic proteins of the Bcl-2 family (Mcl-1, $Bcl\text{-}x_L$, and Bcl-2) because their expression is regulated by HIF-1α in nonmalignant and malignant cells. Moreover, they play a key role in preventing apoptosis mediated by reactive oxygen species (ROS) [14,29–35]. We demonstrated that expression of Mcl-1, $Bcl\text{-}x_L$, and Bcl-2 was significantly inhibited by high AA in K562 cells but was sustained at a higher level in K562-HIF1α cells, regardless of high AA exposure (Figure 5E). We further assessed the involvement of the pro-oncogenic specificity protein (Sp) transcription factors Sp1, Sp3, and Sp4 in the antileukemic effect of high AA because high AA exhibits anticancer activity towards colon cancer cells. This is due in part to downregulation of Sp transcription factors and Sp-regulated genes, such as *VEGF* [36]. There were significant differences in the expression levels of these molecules between the vehicle-treated K562 and K562-HIF1α cells (Figure 5F). In K562 cells, the expression of Sp1, Sp3, and Sp4 as well as that of VEGF was reduced by high AA (Figure 5F). In K562-HIF-1α cells, the expression of Sp1, Sp3, and Sp4 was reduced by high AA, but the expression of VEGF was not (Figure 5F).

Finally, we mixed K562 or K562-HIF1α cells in basement membrane matrix, transplanted the mixture into mice, and injected the mice intravenously with the vehicle or high AA. We found that administration of high AA repressed tumor neoangiogenesis only in mice transplanted with K562 cells (Figure 6A). Further, administration of high AA significantly repressed the growth of K562 tumors but did not detectably inhibit the growth of K562-HIF1α tumors in mice (Figure 6B).

Discussion

AA plays a key role in protecting cells against oxidative damage. Paradoxically, in the presence of Fe^{3+} or Cu^{2+}, AA treatment generates ROS, such as H_2O_2 [37], and induces apoptosis or necrosis in various malignant cells but not in nonmalignant cells [38]. In the present study, we further investigated these findings and confirmed them using human leukemic and normal hematopoietic cells. We found that high AA induces apoptosis only in the leukemic cells, which we concluded reflects the increasing generation of H_2O_2 and relatively low catalase activities [24,39].

We also found that intravenous administration of high AA repressed proliferation of leukemic cells injected into nude mice. Although high AA are usually given by drip infusion in clinical settings [7,9,40,41], we injected mice with high AA in the form of a bolus, which might have weakened the effect of treatment because of more rapid clearance of AA than by drip infusion [42]. However, we observed a significant antileukemic effect of high AA in the present study. Further, the tumors showed markedly reduced neoangiogenesis. Our present findings demonstrate that high AA strongly inhibits expression of HIF-1α and one of HIF-1α-regulated molecules, VEGF, in leukemic cells. HIF-1α and VEGF are considered as potential targets for cancer therapy because they play an important role in the progression of many types of cancer, including leukemia, and are associated with resistance to therapy and poor prognosis [10–13,43–45]. Wang et al. demonstrated that HIF-1α signaling is selectively activated in human leukemic cells even under normoxic conditions [10]. AA

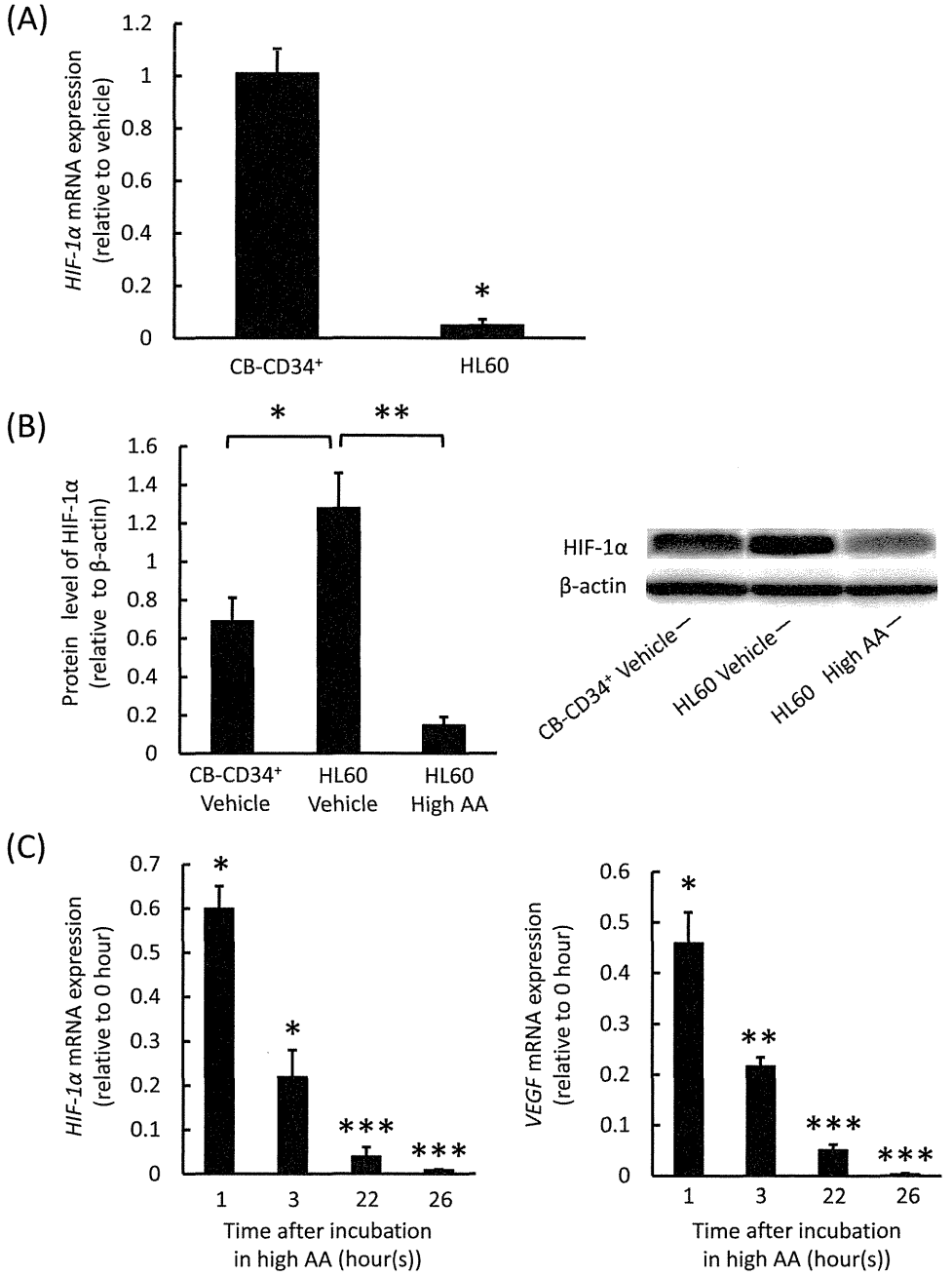

Figure 3. Expression of angiogenesis-related molecules in human leukemic and CB-CD34$^+$ cells exposed to the vehicle or to high AA. A) Quantitative real-time PCR (qRT-PCR) analysis of *HIF-1α* mRNA in CB-CD34$^+$ and HL60 cells. The cells were treated with vehicle or high AA for 1 h, and then washed, cultured, and analyzed after 24 h. There were no significant differences in the expression levels for the 2 conditions ($P>0.05$) in CB-CD34$^+$ cells. In contrast, there were significant differences in the expression levels between the 2 conditions (*$P<0.0001$) in HL60 cells. The values represent the mean ± SD values of triplicate samples. B) Western blotting analysis of HIF-1α in CB-CD34$^+$ and HL60 cells. The cells were treated with vehicle or high AA for 1 h, and then washed, cultured, and analyzed after 24 h. There were significant differences in the expression levels (*$P<0.01$, **$P<0.0005$). The values are mean ± SD values of triplicate samples. C) Sequential analysis of qRT-PCR results of *HIF-1α* and *VEGF* mRNA in HL60 cells. The cells were treated with high AA for 1 h, and then washed, cultured, and analyzed after 1, 3, 22, and 26 h. The expression of *VEGF* mRNA reduced along with that of *HIF-1α* over time. Compared with the expression levels at 0 h, there were significant differences in the expression levels (*$P<0.01$, **$P<0.001$, ***$P<0.0001$). The values represent the mean ± SD values of triplicate samples.
doi:10.1371/journal.pone.0062717.g003

facilitates the hydroxylation of HIF-1α via the stimulation of the Fe-dependent hydroxylases that mark this protein for polyubiquitination and subsequent proteosomal degradation [19,20]. Moreover, Knowles et al. reported that AA reduces HIF-1α protein levels in several human non-hematopoietic cancer cells under normoxic conditions [46]. We have shown here that high AA markedly inhibits the expression of HIF-1α at the level of transcription in leukemic cells.

We have also shown here that in the leukemic cells, high AA inhibited *HIF-1α* transcription by blocking transcriptional activa-

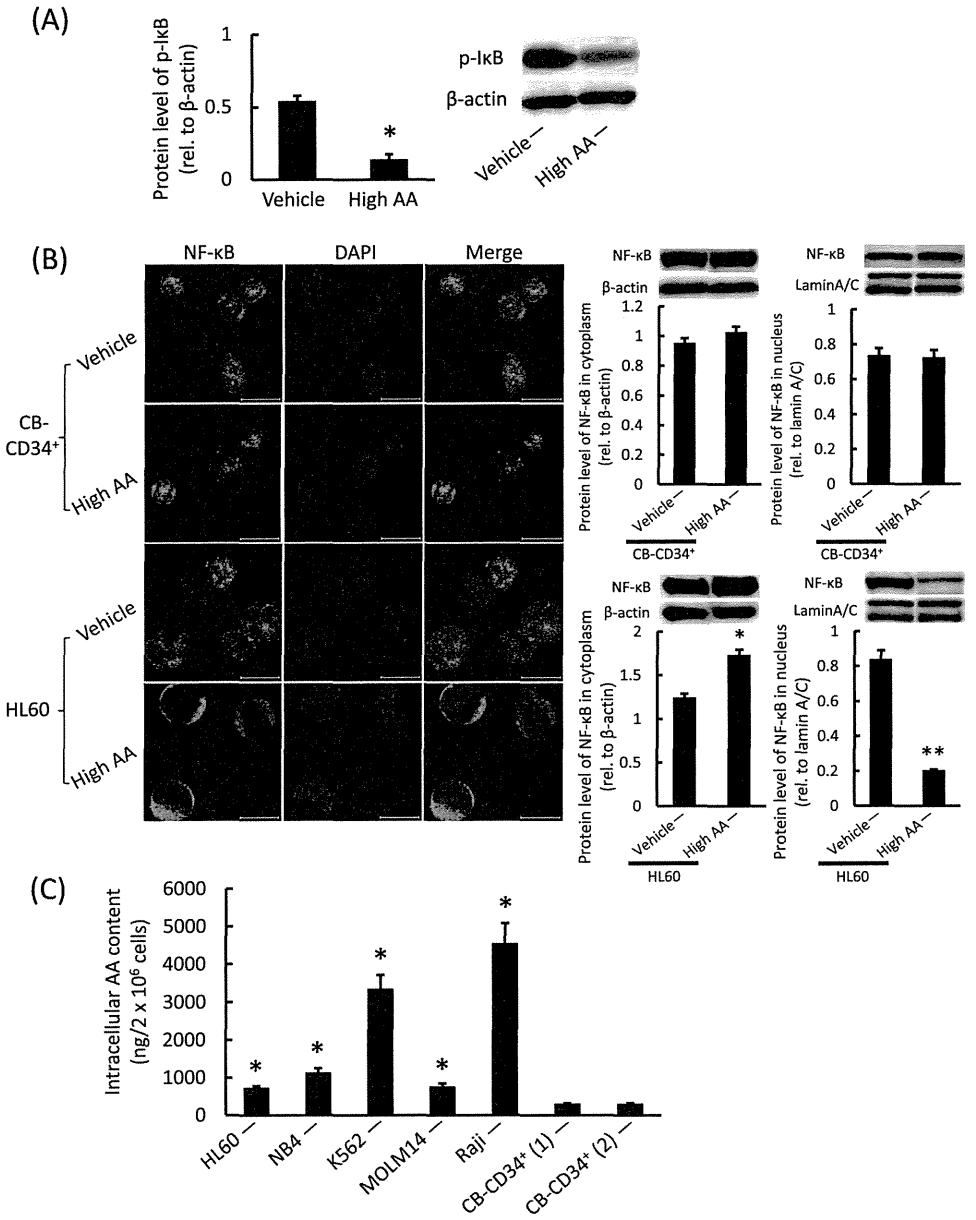

Figure 4. Differences in NF-κB activation and intracellular AA content between human leukemic and CB-CD34$^+$ cells in the presence of high AA. A) Western blotting analysis of p-IκB in HL60 cells. Cells were treated with the vehicle or with high AA for 1 h, and then washed, cultured, and analyzed after 24 h. There was a significant difference in the expression levels (*$P<0.001$). Values represent the mean ± SD of triplicate samples. B) Immunocytochemical (left) and Western blotting (right) analyses of NF-κB in CB-CD34$^+$ and HL60 cells. Cells were treated with vehicle or high AA for 1 h, then washed, cultured, and analyzed after 24 h. Note that translocation of NF-κB into the nucleus was markedly decreased in high AA-treated HL60 cells. Green and blue signals represent NF-κB and DAPI, respectively. Bars indicate 20 μm. There were significant differences in the expression levels (*$P<0.001$, **$P<0.0001$). The values represent the mean ± SD values of triplicate samples. C) Intracellular AA content of human leukemic cells and 2 different isolates of CB-CD34$^+$ cells. Cells were treated with high AA for 1 h, washed in PBS, and analyzed immediately. There were significant differences in the content between leukemic and CB-CD34$^+$ cells. *$P<0.001$, as compared with CB-CD34$^+$ cells (1) or (2). The values are mean ± SD values of triplicate samples.
doi:10.1371/journal.pone.0062717.g004

tion of NF-κB, which is also constitutively activated in many types of leukemia and is associated with leukemic progression [47–49]. Because the leukemic cells used in this study generally possessed significantly higher intracellular levels of AA than normal hematopoietic cells after incubation with high AA, we speculate that while H_2O_2 acts to activate NF-κB by increasing phosphorylation of IκB and *HIF-1α* expression [15,28], AA overcomes the effect of H_2O_2 on the regulation of NF-κB activation in the leukemic cells. Further, we conclude that the increased uptake of AA by leukemic cells, also observed by other investigators and possibly associated with an abnormality in AA transport [50–52], reflects the difference in HIF-1α expression levels between leukemic and normal CB-CD34$^+$ cells after high AA exposure. The levels of intracellular AA did not closely correlate with the cytotoxic effects of high AA, as shown in Figures 1A and 4C,

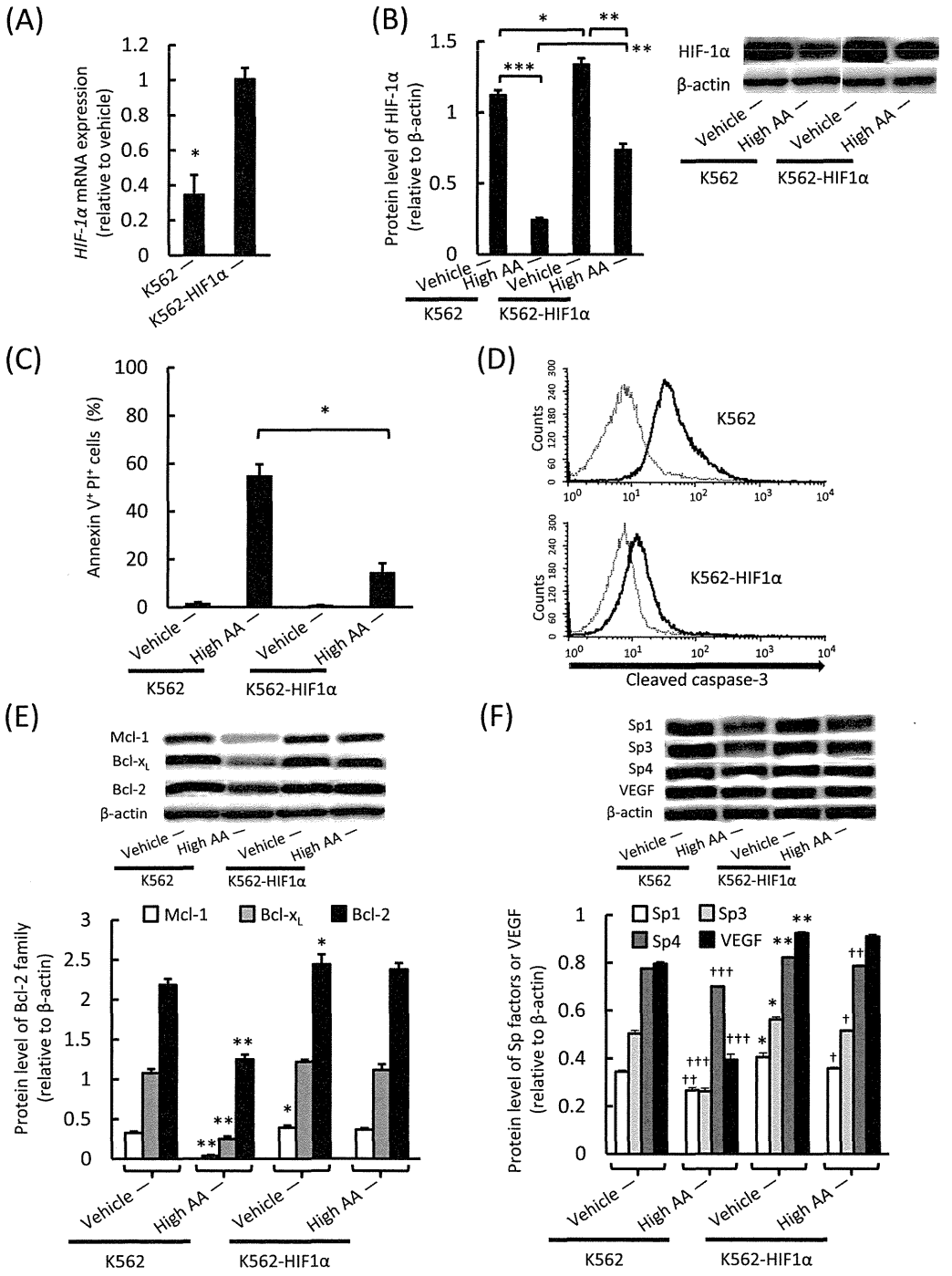

Figure 5. Relationship between antileukemic effects of high AA and HIF-1α expression. A) Quantitative real-time PCR analysis of *HIF-1α* mRNA expression in K562 and K562-HIF1α cells. Cells were treated with the vehicle or high AA for 1 h, washed, cultured in the medium, and analyzed after 24 h. After high AA exposure, *HIF-1α* mRNA expression significantly reduced in K562 (*$P<0.01$), but not in K562-HIF1α cells ($P>0.05$). The values represent the mean ± SD values of triplicate samples. B) Western blotting analysis of HIF-1α in K562 and K562-HIF1α cells. Cells were treated with vehicle or high AA for 1 h, washed, cultured in the medium, and analyzed after 24 h. High AA exposure significantly reduced the HIF-1α protein level in both types of cells. However, the HIF-1α protein level in K562-HIF1α cells was significantly higher than that in K562 cells after vehicle or high AA exposure. *$P<0.01$, **$P<0.0001$, ***$P<0.00001$. The values represent the mean ± SD values of triplicate samples. C) Flow cytometric measurement of apoptosis of K562 and K562-HIF1α cells. Cells were treated with vehicle or high AA for 1 h, washed, cultured in the medium, and analyzed after 18 h. There was a significant difference in the number of apoptotic (annexin V^+ propidium iodide $(PI)^+$) cells between high AA-treated K562 and K562-HIF1α cells (*$P<0.001$). The values represent the mean ± SD values of triplicate samples. D) Flow cytometric measurement of cleaved caspase-3 expressed by K562 and K562-HIF1α cells. Cells were treated with vehicle (gray lines) or high AA (black lines) for 1 h, washed, cultured, and analyzed after 24 h. Activation of caspase-3 by high AA was lower in K562-HIF1α than in K562 cells. E) Western blotting analysis of Mcl-1, Bcl-x_L, and Bcl-2 in K562 and K562-HIF1α cells. Cells were treated with vehicle or high AA for 1 h, washed, cultured, and analyzed after 24 h. There were significant differences in the expression levels between the vehicle-treated K562 and K562-HIF1α cells (*$P<0.05$) and between the vehicle-treated and high AA-treated K562 cells (**$P<0.0001$). There was no significant difference between the vehicle-treated and high AA-treated K562-HIF1α cells ($P>0.05$). The values